THEORETICAL STUDIES OF TRANSPORT AND SURFACE PROPERTIES OF LIQUID Fe−Mn AND Fe−Co ALLOYS

BY

SAMUEL OLUGBADE OGUNDEJI (B.Tech., LAUTECH)

(20164026808)

A THESIS SUBMITTED TO THE POSTGRADUATE SCHOOL, FEDERAL UNIVERSITY OF TECHNOLOGY, OWERRI

IN PARTIAL FULFILMENT OF THE REQUIREMENTS FOR THE AWARD OF THE DEGREE OF MASTER OF SCIENCE (M.Sc.) IN SOLID STATE PHYSICS

FEBRUARY, 2020.

CERTIFICATION

This is to certify that this work "Theoretical studies of transport and surface properties of liquid Fe-Mn and Fe-Co alloys" was carried out by I, SAMUEL OLUGBADE OGUNDEJI (20164026808) in partial fulfilment for the award of the degree of M.Sc. in Solid State Physics in the Department of Physics, Federal University of Technology, Owerri.

.....	17/02/2020
Prof. B.C. Anusionwu.	Date
(Supervisor)	
.....	17/2/2020
Prof. (Mrs.) C.A. Madu.	Date
(Co-supervisor)	
.....	17/2/2020
Prof. (Mrs.) C.A. Madu.	Date
(H.O.D, Dept. of Physics)	
.....	18/2/2020
Prof. C.C.Z. Akaolisa.	Date
(Dean, SOPS)	
.....	.....
Prof. (Mrs.) N.N. Oti.	Date
(Dean, Postgraduate School)	
.....	04/02/2020
Prof. B.A Ezekoye.	Date
(External Supervisor)	

DEDICATION

This work is dedicated to my loving parents.

ACKNOWLEDGEMENT

I would like to express sincere gratitude to my supervisor, Prof. B.C. Anusionwu for his interest, support and guidance throughout the course of this work. Despite his busy schedules, he created time for this work which has led to its successful completion.

I equally want to sincerely appreciate my co-supervisor and Head, Department of Physics, Prof. (Mrs.) C.A. Madu for providing an enabling environment for the PG programme. I also appreciate her invaluable contributions, guidance and suggestions during the course of this work.

The efforts of the PG coordinator, Department of Physics, Dr. K.B. Okeoma during the course of the programme are appreciated. I also appreciate the lecturers, technologists and administrative staff in the Department of Physics for their help and support.

I want to thank Prof. O.E. Awe of the Department of Physics, University of Ibadan for his contributions to this work.

I would like to thank Mr. Sebastine Okoro who was of help in installing the Linux Mint operating system, the environment where all the calculations in this work were carried out. I want to appreciate my colleagues- Mr. James Ezihe and Mr. Valentine Ihejirika for the useful thoughts we shared together during the course of this programme.

I would like to thank my friends and other people who have been of immense help and support while running this programme.

I am greatly indebted to my parents- Mr. O.A. Ogundeji and Mrs. R.O. Ogundeji for their moral and financial supports from my elementary school up till now. I also want to sincerely appreciate my siblings- Ibukun, Iyanu and Promise for their love and care.

Finally and above all, I am grateful to the Almighty God from whom all blessings flow.

TABLE OF CONTENTS

LIST OF TABLES

LIST OF FIGURES

ABSTRACT

Transport and surface properties of liquid Fe−Mn and Fe−Co alloys were computed using the self-association model in conjunction with a model based on the hard-sphere theory, the model of Moelwyn-Hughes and a statistical mechanical approach. Using the self-association model, the model parameters were determined from the experimental thermodynamic data at 1863 K. These model parameters were then used to compute the concentration-concentration fluctuations at the long wavelength limit ($S_{cc}(0)$), short range order parameter (α_1), mutual diffusivity, viscosity, surface concentration, surface tension and surface $S_{cc}(0)$ for the two alloys at 1863 K. Results obtained show that Fe−Mn alloy with low tendency of homocoordination exhibits ideal mixing below 0.25 and above 0.88 atomic fractions of iron. On the other hand, Fe−Co alloy shows ideal mixing property below 0.20 and above 0.88 atomic fractions of iron, homocoordination between 0.20 and 0.70 atomic fractions of iron (Fe) and weak ordering between 0.70 and 0.90 atomic fractions of iron (Fe). Throughout the entire concentration range, diffusion-related activities as reflected by mutual diffusivities are higher in Fe−Mn alloy than in Fe−Co alloy. The viscosities of the two liquid alloys exhibit negative deviations from Arrhenius' law, with the negative deviation being more pronounced in the Fe−Co alloy. Calculations also indicate that more Mn-atoms segregate at the surface of Fe−Mn alloy whereas nearly equal concentrations of Fe-atoms and Co-atoms are at the surface of Fe−Co alloy. These observations possibly suggest that more Fe-atoms are present at the surface of Fe−Co alloy than that of Fe−Mn alloy. The surface tension of Fe−Mn alloy increases throughout the entire concentration range while for Fe−Co alloy, it initially decreases to around 0.59 atomic fraction of iron (Fe) before it rises rapidly. The results from the computation of surface concentration-concentration fluctuations at the long wavelength limit corroborate the results from bulk properties calculations.

Keywords: Mutual diffusivity; Viscosity; Surface concentration; Surface tension; Fe−Mn alloy; Fe−Co alloy; Homocoordination; Ideal mixing.

CHAPTER ONE

INTRODUCTION

1.1 Background information

Matter exists in four different states. They are solid, liquid, gas and plasma. The molecules in a liquid are freer to move around because they are being held together by intermolecular forces that are weaker than those in solids. Like in solids, the liquid molecules are closely-packed together but are free to move around randomly. Therefore, a liquid is able to flow like gas but does not disperse to fill every shape of the container. It has no specific shape but it always takes the shape of the object in which it is contained. It has definite volume and can be poured.

Atoms in liquids do not form a crystalline lattice as in solids and they do not move far apart from each other as in gases. Atoms in the liquid state are randomly distributed and arranged in a nearly close-packed structure. Therefore, due to high packing density there is some degree of short-range order in liquids, but they have long-range disorder due to thermal excitation and motion (Iida & Guthrie, 1988). Thus, liquids do not show any form of long-range order. This is clearly shown with the absence of Bragg peaks in the studies of X-ray and neutron diffraction.

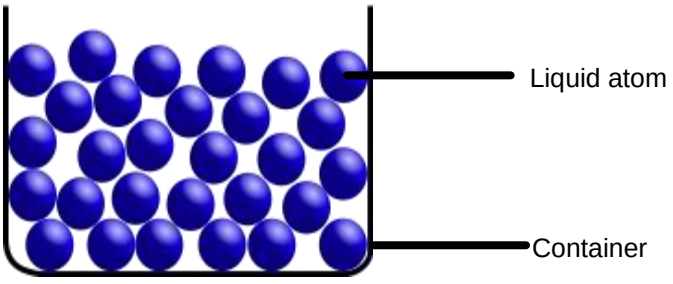

Figure 1.1: Structure of a classical monoatomic liquid (“Liquid,” n.d.)

The study of the liquid state of matter is not as easy and direct as that of solids and gases. By the early nineteenth century there have been established theories on the properties and characteristics of the ideal crystalline solids and the ideal gases (Iida & Guthrie, 1988). Experimental as well as theoretical methods have been used in studying ideal solids and gases and a great amount of knowledge has been gained (Iida & Guthrie, 1988). The structures and properties of liquids are still not understood perfectly as in the solid and gaseous states. This is because the liquid state has no "ideal model" on which a base can be formed.

An ideal model is a hypothetical substance which has the characteristic features of a real matter. Ideal models play a vital role in the study of the properties of matter because they are simple to treat mathematically and their concepts are clear. Solids and gases have ideal models. Ideal models make the study of the solid and gaseous states easier and more direct than that of the liquid state.

For a solid, the ideal model is a perfect crystal in which the atoms at the lattice points are arranged in a regular pattern. This regular arrangement of atoms in three-dimension is long-ranged and undisturbed by thermal agitation. The ideal solid has a crystal of invariant shape.

On the other hand, an ideal gas is the ideal model for the gaseous state of matter. In the ideal gas, each atom is free to move throughout the volume in which it is contained. For real solids and gases, these ideal models yield useful results. Examples are Einstein formula for specific heat, the Brillouin zone, Boyle's and

Charles laws etc. Providing extensions and corrections for the description of real substances can lead to close agreement with experiments (Iida & Guthrie, 1988).

Providing an ideal model for the liquid is a very difficult task. This makes it quite difficult to explain the behavior of a liquid. Microscopically, a liquid is not able to support any form of deformation because of its capacity to flow. Therefore, liquids have very low viscosities and very high diffusivities when compared with the same properties in solids. This suggests that an atom in the liquid state can easily move through fluctuations in density due to the thermal motion of surrounding atoms. If an atom in the liquid state is considered at any moment, it will be interacting with the surrounding atoms, vibrating as though it were an atom in the solid state. At the next moment its behaviour may change to that of an atom in the gaseous state, and move freely. Therefore, to have a proper understanding of the structures and properties of liquids, both atomic distance and time scales are of great importance (Iida & Guthrie, 1988).

Liquids can be divided into two categories. They are simple and complex liquids. Simple liquids are liquids with one component atom. Examples are metallic liquids. As the number of atom types in a liquid increases, the liquid complexity increases. Water is a complex liquid.

Liquids from pure metals serve as the simplest form of liquids because they are mono-component and one form of interaction may exist among the atoms. Liquid metals are a group of non-crystalline metal alloys. They are referred to as liquid metals because they retain their non-crystalline liquid structure on cooling from

melt. Being the simplest forms of liquid state, researchers have shown interest in studying the properties of liquid metals. Alloys of liquid metals have some desirable properties which include high tensile strength, electrical and thermal conductivities, excellent wear and corrosion resistance and very high coefficient of restitution. A few elemental metals are liquids at or near room temperature. The commonest is mercury (Hg), which is molten above 234.3 K. Others are gallium (Ga) with a melting point of 301.1 K, caesium (Cs) with a melting point of 301.7 K, rubidium (Rb) with a melting point of 312 K and francium (Fr) with a melting point of 300.1K.

Some metals on their own do not possess all the necessary properties required for a particular application. By forming alloys, one can obtain increased strength and other desirable properties. Generally, metal alloys have advantages over metals in different engineering and metallurgical processes. Some of these advantages include increased mechanical strength, corrosion resistance, heat resistance, increased abrasion, a wide range of colours and reduced costs of production. Alloys are used in making some jewellery, coins, bridges, nails, screws, tanks, drinks cans, artificial joints, bicycles, car bodywork etc.

Liquid alloys have disordered structure and short-range order. Disordered materials such as liquid alloys are not easy to study as those of crystals (Koirala, Singh, & Jha, 2014). Liquid alloy properties have been a subject of interest to researchers based on the interactions between the atoms (or molecules) of the alloys (Bhatia, Hargrove, & March, 1973; Butler, 1932; Faber, 1972; Flory, 1942; Guggenheim, 1952; Novakovic, 2010; Singh, Mishra, & Singh, 1990; Singh & Sommer, 1992). Thermo-physical properties of binary liquid alloys are difficult and expensive to determine

from experiments. This is because some alloy systems may be chemically active. Also, experimental determination of properties such as diffusion, viscosity and surface tension are quite difficult and costly at elevated temperatures. On the other hand, theoretical methods reduce the time and efforts required in the determination of these thermo-physical properties. As a result theoretical models are very important in studying the properties of liquid alloys.

Thermodynamic, structural, transport and surface properties of binary liquid alloys can be computed in order to study their alloying behaviour. Thermodynamic properties such as Gibbs free energy of mixing (G_M), activity (a), entropy of mixing (S_M) and enthalpy of mixing (H_M) help to understand the interaction, stability and bonding strength among the component atoms in an alloy (Koirala, Jha, & Singh, 2014). They are defined below:

Gibbs free energy of mixing (G_M): This is the greatest amount of mechanical work that is obtainable from a given quantity of a substance.
Activity (a): This is defined as a measure of tendency of an alloy component to leave the solution.
Entropy of mixing (S_M): This represents the degree of disorderliness in the local arrangement of atoms in a system.
Enthalpy of mixing (H_M): This is the amount of heat absorbed or given out by a substance upon mixing.

Accurate knowledge of phase diagrams and thermodynamic quantities of alloys is pivotal to getting a reliable result from theory (Ajayi, Ogunmola, & Adeoye, 2017). Some thermodynamic measurements serve as inputs for many of the theoretical

models used in studying transport and surface properties of liquid alloys (Anusionwu, Madu, & Orji, 2009). Thus, thermodynamic properties are important in studying binary liquid alloys.

Concentration-concentration fluctuations at the long wavelength limit, $S_{cc}(0)$ and Warren-Cowley (Cowley, 1950; Warren, 1969) chemical short range order parameter, α_1 are very useful for obtaining microscopic information such as local ordering and segregation in liquid alloy systems (Singh, 1987). These two parameters help to shed light on the local arrangement of atoms in binary liquid alloys.

The concentration-concentration fluctuations at the long wavelength limit, $S_{cc}(0)$ is useful in shedding light on the phenomenon of homocoordination (i.e. pairing of like atoms as nearest neighbours) and heterocoordination (i.e. pairing of unlike atoms as nearest neighbours) (Prasad, Singh, Singh, & Chatterjee, 1995). In addition, concentration-concentration fluctuations at the long wavelength limit, $S_{cc}(0)$ is important in determining the short range order parameter and mutual diffusivities of binary liquid alloys. The values of α_1 give the strength of the local arrangement of atoms in a binary alloy (Koirala, Singh, Jha, & Adhikari, 2013).

Alloys have transport properties (e.g. diffusion and viscosity) which make them fit for various applications. A good knowledge of transport properties of liquid alloys is required in various heterogeneous chemical reactions and metallurgical processes (Koirala *et al*., 2014). Transport quantities affect a lot of technological processes and

corrosion phenomena and as well contribute to the amount of knowledge we have about liquids (Schwitzgebel & Langen, 1981).

Diffusion is defined as the mass transport process from one point to another at the microscopic level. Liquid state diffusivities are higher than those in the solid state. For metals, diffusivities in both states differ by a factor of 10^2 to 10^3 (Iida & Guthrie, 1988). Diffusivity has been a subject of interest in science and technology. Adequate knowledge of diffusivities in liquid alloys is useful when designing metallurgical and solidification processes (Dalgic & Colakogullari, 2006).

On the other hand, viscosity is the fluid's resistance to flow. It is a physical property which can only be observed when a relative motion is set up between different layers of a fluid. Microscopically, it is a measure of the friction that exists among atoms of a fluid. Viscosity is very important in the technology and theory of liquid metal because it plays a significant role in solving problems in fluid flow behaviour and those related to the kinetics of reaction in metallurgical processes (Iida & Guthrie, 1988).

Adequate knowledge of surface segregation and surface tension is essential in material processing and metallurgical processes. Surface segregation takes place whenever the surface of a binary liquid alloy is enriched by the atoms of a constituent element (Prasad, Singh, Singh, & Singh, 1998). Also, surface segregation is the difference between surface and bulk concentrations (Prasad & Singh, 1991).

On the other hand, surface tension is the property of a liquid in which the surface acts as though covered with an elastic skin. It is the work or energy required to create one unit of additional surface area at constant temperature (Iida & Guthrie, 1988). An understanding of metallurgical processes requires the knowledge of surface tension. The surface tension of a liquid metal influences phenomena and technologies such as casting, brazing, sintering, zone melting and fibre formation (Iida & Guthrie, 1988).

In a binary liquid alloy, whenever there is a reasonably large difference in the surface tension values of the alloy components, the component having a small value of surface tension will have a strong segregation at the surface while the other component will prefer to remain in the bulk (Koirala, Kumar, Singh, & Adhikari, 2014). However, when the surface tension values of the metals are very comparable, there is no much difference between the surface concentrations and the bulk concentrations (Koirala *et al.*, 2014).

Proper understanding of phenomena such as corrosion, welding, casting, gas absorption, welding characteristics of solders, kinetics of phase transformation, heterogeneous catalysis, epitaxial growth and wettability at weld joints requires the knowledge of surface properties (Anusionwu, 2003; Prasad & Singh, 1991).

1.2 Problem statement

A lot of experiments have been carried out on transport properties (e.g. diffusion and viscosity) and surface properties (e.g. surface tension) yet the available data are

scanty. In addition, some of the available data are not of sufficient accuracy. This may be due to the fact that experimental measurements of these properties at elevated temperatures is not a simple task. At elevated temperatures where most metals become liquids it will be difficult to experimentally measure these transport and surface properties.

The need to study these properties at elevated temperatures necessitates the use of theoretical models. Theoretical models reduce the time, efforts and costs in determining transport and surface properties of liquid alloys.

1.3 Objectives of study

The aim of this study is to theoretically study the transport and surface properties of liquid $Fe - Mn$ and $Fe - Co$ alloys at $1863\ K$.

The objectives of this study are to:

i. Compute for the liquid $Fe - Mn$ and Fe−Co alloys thermodynamic properties and compare with experimental values at 1863 K.
ii. Compute the values of self-diffusivity, viscosity and surface tension of iron (Fe), manganese (Mn) and cobalt (Co) at 1863 K.
iii. Compute for the liquid $Fe - Mn$ and Fe−Co alloys the order, mutual diffusivity, viscosity, surface concentration, surface tension and surface concentration-concentration fluctuations at the long wavelength limit, $S_{cc}^{s}(0)$ at 1863 K.

1.4 Justification of study

This study will help in predicting the values of self-diffusivities, viscosities and surface tension of Fe, Mn and Co at 1863 K, a temperature which is higher than their melting points. The study will also help to predict the mutual diffusivities, viscosities, surface concentration, surface tension and surface $S_{cc}(0)$ for liquid Fe−Mn and Fe−Co alloys at $1863\ K$.

In order to properly understand the nature of Fe−Mn and Fe−Co alloys in the solid state, the knowledge of their alloying behaviour in the liquid phase is important. This is because most solid alloys are gotten from their respective liquid state. The current interest in liquid Fe−Mn and Fe−Co alloys is due to the improved and desirable properties they have and their interesting applications in solid state in various fields (Bloch, Waeckerle, & Fraisse, 2007; Drynda, Hassel, Wilhelm & Peuster, 2014; Gasior, Fima, & Moser, 2011; Koirala *et al*., 2014; Lee *et al*., 2017; Liu, Bauser, Turgut, Coate, & Fingers, 2003; Varadaraajan, 2015).

1.5 Scope of study

The self-association model of Singh and Sommer (1992) will be used to compute the Gibbs free energy of mixing and activity of the liquid Fe−Mn and Fe−Co alloys at 1863 K. Through this model, the values of n (ratio of self-associate) and W/RT (order energy parameter) would be obtained from the experimental thermodynamic data at $1863\ K$.

The optimised model parameters ($n, W/RT$), will then be used to compute activity coefficients, bulk $S_{cc}(0)$ and (α_1). These quantities will serve as inputs when computing transport and surface properties of Fe−Mn and Fe−Co alloys at 1863 K in the entire concentration range

CHAPTER TWO

LITERATURE REVIEW

2.1 Properties and uses of iron

Iron (Fe) belongs to the family of transition metals. The atomic number of iron is 26. It is known to be the most important and widely used of all metals. It is a shiny, greyish metal that rusts easily in moist air but it is mostly used because it is cheap. Pure iron is soft, very malleable and has magnetic properties.

Commercial production of iron can be done in a blast furnace by addition of heat to haematite or magnetite with carbon and limestone. This forms pig iron which has about 3% carbon and other impurities. Iron is the main material needed for the production of steel. The strength of iron is enhanced once it is made into steel. The quantity of crude steel produced yearly all over the world is about 1.3×10^9 tonnes ("Periodic table," n.d.).

Figure 2.1: Iron ("A chunk of iron", n.d)

2.2 Properties and uses of manganese

Manganese (Mn) is a silvery-grey, hard and brittle transition metal with atomic number 25. It is similar in appearance to iron but is harder and more brittle. It is the second most abundant transition metal and has paramagnetic properties.

Manganese is a metal which can be used to produce very hard steels. If steel is produced without alloying with manganese, it breaks up easily when hot-rolled or forged ("Manganese," n.d.). Manganese is commonly used in low-alloy steels due to its effect in increasing hardenability and decreasing softening on tempering (Nasim, 1979). Manganese steel which is also known as Hadfield steel (containing 11-14% manganese) is used for services that require ruggedness. In steel production, manganese helps to remove certain impurities like sulphur and oxygen and adds essential physical properties to steel (Downing, n.d.). As an alloy agent in steel, it helps to improve strength, hardness, hardenability (Senk, Emmerich, Rezende, & Siquieri, 2007). As a pure metal, it is added to non-ferrous alloys such as copper, aluminum, magnesium and nickel.

Carbon steels with manganese added are stronger and tougher. Materials made of steel are used for various purposes. Such steels possess a variety of applications in cutting tools, bicycle chains, bridges, electricity pylons, railway tracks and gun barrels, etc. Manganese steels possess interesting combination of properties and are cheap.

Figure 2.2: Manganese (“Manganese,” n.d.)

2.3 Properties and uses of cobalt

Cobalt is a transition metal with atomic number 27. It is a silvery, shiny and brittle metal used in the production of permanent magnets and alloys that are resistant to corrosion and heat. It is a naturally occurring magnetic metal like nickel and iron. Of all metals, its Curie temperature is the highest and this makes it to retain its magnetism at a high temperature.

Figure 2.3: Cobalt (“Cobalt,” n.d.)

2.4 Alloys of iron

An alloy is a metal which contains two or more elements, at least one of which is a metal. It is an industrial material that is grown from molten state. Examples of alloys include steel (Fe−C), brass (Cu−Zn), Fe−Si, Cd−Ga, Mn−Cu, etc.

Iron is an important metal and one of the most widely used in industries. Alloying it with elements such as manganese, cobalt, nickel, chromium, silicon, aluminium etc., will produce materials with improved and desirable properties.

2.4.1 Fe−Mn alloys

Fe−Mn alloys have special properties such as resistance to heat and corrosion, non-magnetic characteristics etc. These properties make them to be widely used in rolled products. Fe−Mn alloys have applications in mining, construction and transportation industries. Since it was discovered by Sir Robert Hadfield, Fe−Mn−C alloy has been of interest to researchers because it has high mechanical properties (ductility and strength).

The use of manganese has been mainly in low alloy steels and Hadfield's manganese steel. Because of its abundance, low cost and similarities with nickel, it has been studied by many researchers as a replacement for nickel in high alloy steels (Bramhall, 1989). Binary Fe−Mn alloy is brittle and this has limited its use as a cryogenic steel (Nasim, 1979).

Due to the large chromium content ranging from 15−25% in the Fe−Ni matrix, commercial austenitic stainless steels are good ductile metals with excellent resistance to corrosion and high temperature stability (Bramhall, 1989). Austenite Cr−Ni stainless steels are known for cryogenic and non-magnetic applications but the material cost is high when compared to austenitic high manganese steels (Bramhall, 1989). Manganese forms austenite and is cheaper compared to nickel. Austenite-forming Fe–Mn alloys can serve as replacements for the known Fe–Cr−Ni alloys, where manganese can be substituted for nickel and chromium (Hermawan, Alamdari, Mantovani, & Dube, 2008).

Enhanced strength, improved wettability, good machinability and low magnetic permeability are required for non-magnetic structural applications while low temperature toughness is required for cryogenic applications like superconducting technology and storage and transportation of liquid natural gas (Bramhall, 1989).

Charles and Issi (1984) studied the electrical and thermal conductivities of binary Fe−Mn and ternary Fe−Mn−Al austenitic alloys. They found that adding aluminium to Fe-Mn austenitic alloys strongly affected the transport properties. The electrical resistivity increased rapidly while the thermal conductivity decreased. The reduction in thermal conductivity implies that high manganese austenitic alloys are useful in low temperature (cryogenic) applications.

Varadaraajan (2015) studied the influence of aluminium, chromium and carbon on Fe−Mn alloy so as to increase its resistance to wear and corrosion. He found that the resistance to wear of the alloy is better than that of conventional steels. The alloy

has improved mechanical properties due to various deformations occurring in it (Varadaraajan, 2015). Austenitic Fe−Mn alloys have low cost and are wear-resistant materials which are commonly used in automotive industries (Varadaraajan, 2015).

The binary Fe−Mn and ternary Fe−Mn−C alloys have a good combination of ductility and strength. The corrosion rate in these materials is lowered because manganese is present in them (Opiela, Grajcar, & Krukiewicz, 2009).

Fe-Mn alloys can also be used as biomaterials for medical implants (Drynda *et al.*, 2014; Hermawan *et al*., 2008; Hermawan, Purnama, Dube, Coute & Mantovani, 2010). Biodegradable stents are a possible substitute for the treatment of heart-related diseases. The materials to be used as stents must have excellent mechanical and corrosion properties without producing harmful effects (Hermawan *et al*., 2010). Several attempts have been made to develop stents with alloys of iron. The interest in Fe−Mn alloy is because its corrosion rate can be increased which is a good factor to be considered when developing biodegradable materials (Drynda *et al*., 2014).

Drynda *et al.* (2014) developed new Fe−Mn alloy systems lower concentrations of Mn ($Fe-Mn$ 0.5 wt %, $Fe-Mn$ 2.7 wt %, $Fe-Mn$ 6.9 wt %) in order to prevent toxicity. The alloys they worked on exhibited good mechanical and corrosion properties.

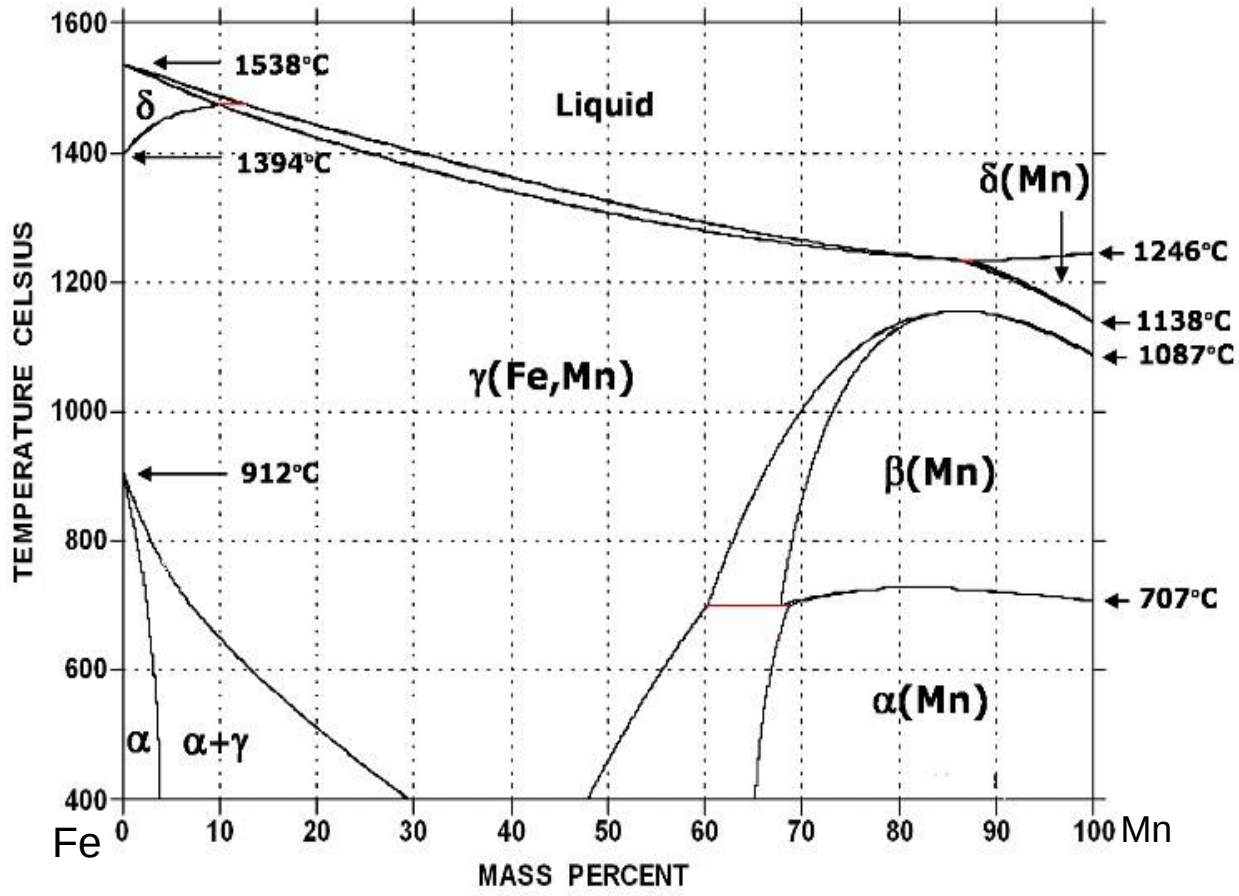

Figure 2.4: Fe−Mn phase diagram ("Iron-Manganese (Fe-Mn) Phase Diagram," n.d.)

Figure 2.4 indicates the phases to be expected at equilibrium for different combinations of manganese contents and temperature.

2.4.2 Fe−Co alloys

Iron and cobalt are two of the three elements (the other being Nickel) that can be used to produce magnetic alloys. The magnetic properties of alloys formed by iron, cobalt and nickel depend on the composition of the alloys, thickness, frequency, stress, heat treatment temperature etc. (Bloch *et al.*, 2007).

There has been considerable interest in binary Fe−Co alloys after Preuss (1912) and Weiss (1912) discovered that alloys of this system (Fe_2Co) have the highest saturation magnetization of ferromagnetic materials. The equiatomic Fe−Co alloy called Permendur was studied and patented by Elmen (1929). He discovered that the alloy possessed excellent magnetic properties. However, it had poor electrical (resistivity) and mechanical (ductility) properties. Also, there was great difficulty in fabricating thin plates of this alloy because it is too brittle.

White and Wahl (1932) proffered solution to this challenge by adding 2% vanadium to the equiatomic Fe−Co alloy to make it easier to cold work. They discovered that adding up to 2% vanadium to the equiatomic Fe−Co alloy did not have much effect on its magnetic properties. But the addition of 2% vanadium greatly improved the electrical and mechanical properties. This caused its electrical resistivity to increase three times and also led to reasonable improvements in ductility, workability and machinability. As a result, thin sheets could be fabricated. This alloy was called 2V-Permendur. Gould and Wenny (1956) named the alloy Supermendur when the base materials for the production of 2V-Permendur are high purity iron and cobalt. They reported that Supermendur had excellent magnetic properties.

Fe−Co alloys are magnetic materials with properties typical of soft or hard magnetic materials (Couto & Ferreira, 1989). In the development of sophisticated power systems, there is the need for the use of soft magnetic materials which have both high mechanical strength and saturation magnetisation (Liu *et al.*, 2003). Since Fe−Co soft magnetic alloys have a good combination of magnetic and mechanical properties, they can be used in magnetic bearings and generators (Fingers & Kozlowski, 1997).

In terms of the surface properties, Vasiliev (1997) found that there was no change in iron (Fe) surface concentration at the surface of equiatomic Co−Fe alloy in the temperature range of 683 to 1123 K. There is no significant iron and cobalt surface segregation of the Co−Fe alloys (Vasiliev, 1997).

Grain size affects the properties of Fe−Co alloys. If the grain size is small, it will have high mechanical properties but the magnetic properties will be low (Bloch *et al*., 2007). The grain size can be increased by using an appropriate heat treatment to obtain a balance between mechanical strength and magnetic performance. This is because a material with large grains would have better magnetic properties than a material with small grains (Liu *et al*., 2003). Therefore, a correct approach to achieving a balance between mechanical and magnetic properties is to increase the grain size (Liu *et al.*, 2003).

Bloch *et al*. (2007) considered iron−cobalt alloys with concentration of cobalt more than 15 %. They found that the alloys have high induction saturation than iron-silicon (Fe−Si) alloy which is the most commonly known of the electrical alloys.

They also found that these alloys can lead to a 30% reduction of the electromagnetic part of an electrical device. They can greatly reduce the magnetic losses in electrical motors, thereby increasing their efficiency. The alloys also have very high Curie temperature that allows their use at very high temperature (Gasior *et al*., 2011; Vasiliev, 1997).

The most commonly used of Fe−Co alloys are the 2V Permendur and the Supermendur alloys. The development of generators and advanced motors for airspace and other special power applications requires light weight, small size, low power consumption, and use of soft magnetic materials which possess high mechanical strength (Couto & Ferreira, 1989). Fe−Co alloys in appropriate concentrations have desirable mechanical and magnetic properties (Gasior *et al*., 2011). These properties are required for advanced power application (Couto & Ferreira, 1989).

Investigations have also been carried out on the use of magnetic alloys for medical applications (Gurrappa, 2002; Mathieu, Martel, Yahia, Soulez, & Beaudoin, 2005; Pouponneau, Savadogo, Napporn, Yahia, & Martel, 2010; Reclaru, Luthy, Eschler, Blatter, & Susz, 2005). As an example, Pouponneau *et al.* (2010) showed that in an experiment performed in the carotid artery of a living swine the magnetic gradients generated by a clinical MRI system could propel and navigate unethered medical microdevices and micronanorobots in the human vasculature.

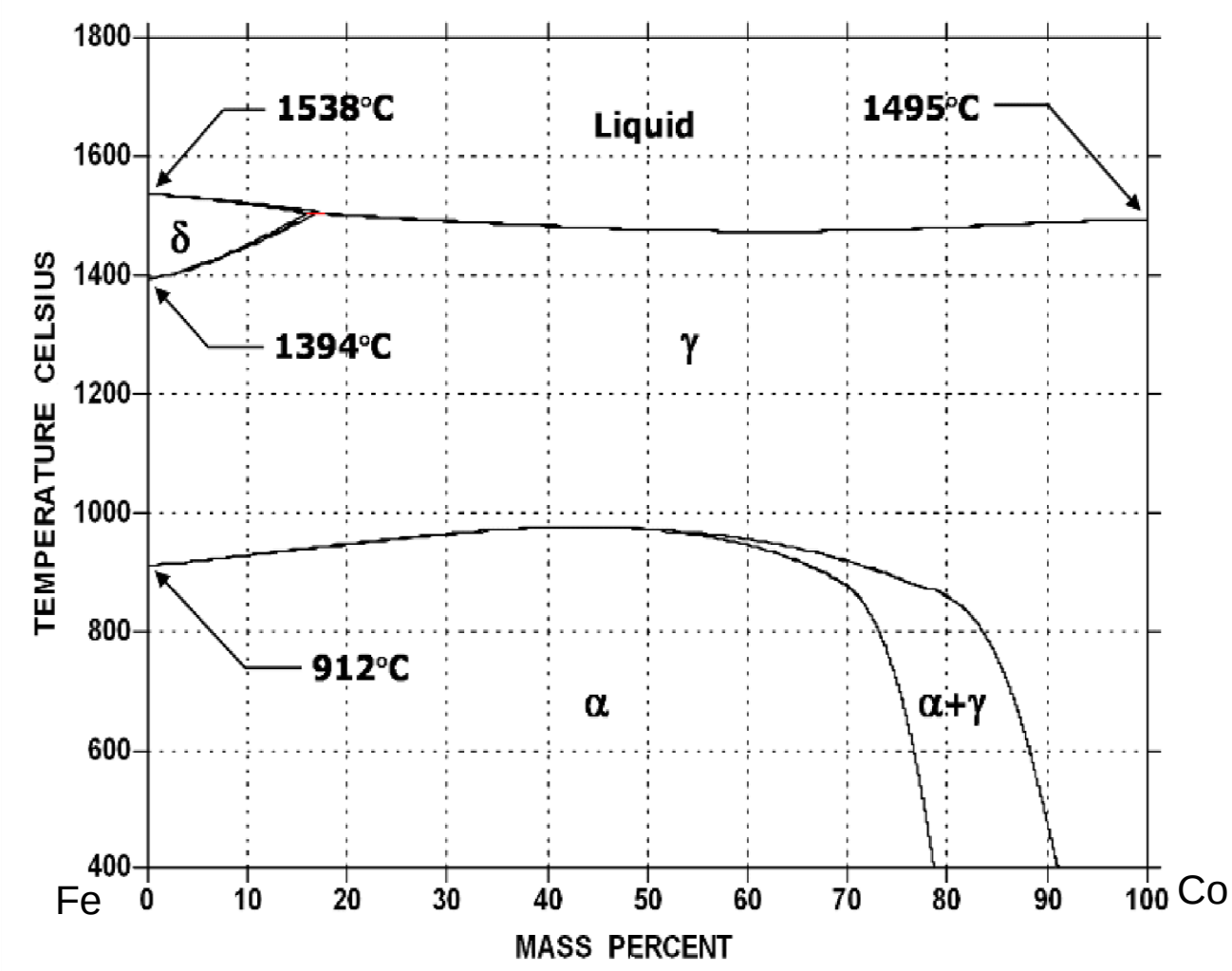

Figure 2.5: Fe−Co phase diagram ("Iron-Cobalt (Fe-Co) Phase Diagram," n.d.)

Fe−Co phase diagram above indicates phases to be expected at equilibrium for different combinations of cobalt content and temperature.

CHAPTER THREE

METHODOLOGY

3.1 Thermodynamic properties

The self-association model was developed by Singh and Sommer (1992). This is a simple statistical model which can be used to study phase segregation in binary liquid alloys. In this model, one assumes that an $A - B$ binary liquid alloy has $N_A = Nc$ atoms of component A and $N_B = N(1 - c)$ atoms of component B, so that the total number of atoms $N = N_A + N_B$. Here c is the concentration of component A. It is further assumed that the elements of the component atoms A and B have the structure of a polyatomic matrix, resulting in the formation of cluster of like-atoms of the kind A_μ and B_ν i.e.,

$$\mu A \rightleftharpoons A_\mu; \qquad \nu B \rightleftharpoons B_\nu, \tag{3.1}$$

In equation (3.1), μ represents the number of atoms in the cluster of matrix of type A while ν represents the number of atoms in the cluster of matrix of type B.

The thermodynamic properties of the demixing liquid alloys are dependent on the number of self-associates,

$$n = \mu/\nu; \qquad \mu > \nu \tag{3.2}$$

Two assumptions are made. The first assumption is that the locations of all the atoms are on a set of equivalent lattice sites and each atom has z nearest neighbours. Secondly, the presence of short-range and effective interaction.

The self-association model gave a simple expression for the Gibbs free energy of mixing as (Singh & Sommer, 1997):

$$G_M = RT[c \ln c + (1 - c) \ln(1 - c) + c \ln(1 - \beta) + \ln \Gamma] + c(1 - c)\Gamma W \tag{3.3}$$

where c is the concentration of atom A.

$$W = \mu w, \;\; \Gamma = \frac{1}{(1-c\beta)} \;, \;\; \beta = 1 - \frac{1}{n} \;, \quad n = \frac{\mu}{\nu} \tag{3.4}$$

In equation (3), w is the order energy or interchange energy. One can use the value of w to deduce the mixing behaviour in alloys. When $w < 0$, it is an indication of heterocoordination (pairing of unlike atoms as nearest neighbours); $w > 0$ is a signature of homocoordination (pairing of like atoms as nearest neighbours); $w = 0$ is an indication of ideal mixing in the alloy.

In addition, computation of thermodynamic properties and microscopic functions of binary alloys at the temperature of investigation requires the fitting of the model parameters n (ratio of self-associates) and W/RT (order energy parameter) at that temperature. The model parameters do not depend on concentration but may be dependent on temperature and pressure (Akinlade, Boyo, & Ijaduola, 1999).

The general expression from which the activities of the components of a binary alloy can be obtained is given as (Anusionwu & Echendu, 2010):

$$RT \ln a_i = \left(\frac{\partial G_M}{\partial N_i}\right)_{T,P,N} , \tag{3.5}$$

Using equations (3.2) and (3.4) and recalling that $N = N_A + N_B$ and $c = N_A/N$, the activities of alloy components are given as (Akinlade *et al*., 1999):

$$\ln a_A = \ln[c\Gamma(1-\beta)] + (1-c)\Gamma\beta + (1-c)^2\Gamma^2 \frac{W}{RT} \tag{3.6}$$

$$\ln a_B = \ln(c\Gamma) + c(1-\beta)\Gamma(1-n) + nc^2(1-\beta)\Gamma^2 \frac{W}{RT} \tag{3.7}$$

where R is the universal gas constant.

The activity coefficients (γ_i) of the alloy components can be obtained from the given expression below:

$$\gamma_i = \frac{a_i}{c_i}, (i = A, B) \tag{3.8}$$

3.2 Structural properties

Theoretical models to determine the concentration-concentration fluctuations in the long wavelength limit $S_{cc}(0)$ and Warren-Cowley short range order parameter α_1 are discussed in this section.

3.2.1 Concentration-concentration fluctuations at the long wavelength limit

The concentration-concentration fluctuations at the long wavelength limit, $S_{cc}(0)$ gives information on the nature of atomic order in an alloy. The concentration-concentration fluctuations at the long wavelength limit, $S_{cc}(0)$ is difficult to obtain from diffraction experiments (x-ray and neutron) (Bhatia, Hargrove, & Thornton, 1974). However, it can be easily determined theoretically from the Gibbs free energy of mixing or activities through the standard relationship (Novakovic, 2011):

$$S_{cc}(0) = RT\left(\frac{\partial^2 G_M}{\partial c^2}\right)^{-1}_{T,P,N} = (1-c)a_A\left(\frac{\partial a_A}{\partial c}\right)^{-1}_{T,P} = ca_B\left(\frac{\partial a_B}{\partial (1-c)}\right)^{-1}_{T,P,N} \tag{3.9}$$

The experimental values of $S_{cc}(0)$ which are not easy to obtain from experiments can be determined from experimental values of activity (Hultgren, Desai, Hawkins, Gleiser, & Kelly, 1973) by using equation (3.9).

By using equations (3.3), (3.6) or (3.7), an expression to determine $S_{cc}(0)$ is given as (Akinlade et al., 1999):

$$S_{cc}(0) = \frac{c(1-c)}{1-c(1-c)g(n,W)} \quad , \tag{3.10}$$

where

$$g(n,w) = \frac{2\,n^2\frac{W}{RT} - (n-1)^2[c+n(1-c)]}{[c+n\,(1-c)]^3} \tag{3.11}$$

As earlier indicated, ideal mixing occurs when the energy parameter, w, in equation (3.4) is zero. Therefore, equation (3.10) reduces to the ideal $S_{cc}(0)$ which is given as (Odusote & Popoola, 2017):

$$S_{cc}(0) = \frac{c(1-c)}{1-c(1-c)(0)} \tag{3.12}$$

The departure of $S_{cc}(0)$ from $S_{cc}^{id}(0)$ can be used to deduce the alloying behaviour of liquid alloys. At a given concentration, a liquid alloy is said to be compound forming if $S_{cc}(0) < S_{cc}^{id}(0)$ while phase separation occurs when $S_{cc}(0) > S_{cc}^{id}(0)$ (Novakovic *et al*., 2012). If $S_{cc}(0) = S_{cc}^{id}(0)$, the alloy shows ideal mixing behaviour (Koirala *et al*., 2013; Anusionwu, Adebayo, & Mbamala, 2013). For a demixing system, $S_{cc}(0) \gg S_{cc}^{id}(0)$ (Boyo, 2005).

3.2.2 Warren-Cowley chemical short range order parameter (α_1)

Warren-Cowley (Cowley, 1950; Warren, 1969) short-range order parameter (α_1) is useful in measuring the degree of chemical order in alloys. Although, it is quite difficult to obtain α_1 from diffraction experiments, it can be determined from the knowledge of $S_{cc}(0)$. Knowledge of α_1 helps to understand the local arrangements of atoms in liquid alloys.

It has been shown that α_1 has values in the following range (Singh, 1987):

$$\frac{-c}{(1-c)} \leq \alpha_1 \leq 1, \quad c \leq 1/2 \tag{3.13}$$

$$\frac{-1(1-c)}{c} \leq \alpha_1 \leq 1, c \geq 1/2 \tag{3.14}$$

For equiatomic concentration ($c = 1/2$), equations (3.12) and (3.13) reduce to

$$-1 \leq \alpha_1 \leq 1 \tag{3.15}$$

There will be complete heterocoordination when α_1 has a minimum value of $\alpha_1^{min} = -1$, complete homocoordination when α_1 has the maximum value of $\alpha_1^{max} = 1$ and random distribution of atoms when $\alpha_1 = 0$ (Akinlade & Singh, 2002).

Singh, Pandey, Sinha, Mistra and Srivastava (1987) have shown that α_1 can be determined from $S_{cc}(0)$:

$$\alpha_1 = \frac{S-1}{[S(Z-1)+1]} \ , \tag{3.16}$$

where

$$S = \frac{S_{cc}(0)}{S_{cc}^{id}(0)} \tag{3.17}$$

Z is the bulk coordination number of the alloy. It has been suggested that the value of Z could be taken as 10 for most of liquid metallic systems (Prasad *et al*., 1995). For this work, Z is taken as 10.

3.3 Transport properties

Transport properties like mutual diffusivity and viscosity are important in understanding the mixing properties of alloys on the atomic scale.

3.3.1 Mutual diffusivity

An important relationship between $S_{cc}(0)$ and diffusivity can be obtained by using Darken (1948) equation for diffusion. This relationship is given as (Singh & Sommer, 1992; Prasad *et al*., 1998):

$$\frac{D_M}{D_{id}} = \frac{S_{cc}^{id}(0)}{S_{cc}(0)} = \frac{c\,(1-c)}{S_{cc}(0)}\ , \tag{3.18}$$

where D_M and D_{id} are the mutual diffusivity and intrinsic diffusivity respectively. The intrinsic diffusivity D_{id} is given as (Prasad *et al*., 1998):

$$D_{id} = cD_B + (1-c)D_A\ , \tag{3.19}$$

where D_A is the self-diffusivity of pure component A, D_B is the self-diffusivity of pure component B and c is the concentration of component A.

The relationship between $S_{cc}(0)$ and diffusivity given by D $(i.e. D_M/D_{id})$ shows the mixing behaviour of alloys. $D > 1$ indicates that there is a tendency to compound formation, $D < 1$ shows phase segregating tendencies and $D \rightarrow 1$ indicates ideal mixing in the alloys (Singh & Sommer, 1992).

Equation (3.18) can be used to calculate the mutual diffusivity for alloys if the experimental self-diffusivities D_i of the alloy components are known. But there are scanty experimental data in the literature. In order to have a clear understanding of diffusion-related phenomena in liquid metals, knowledge of self-diffusivities is required (Iida & Guthrie, 1988). The knowledge of self-diffusivities of liquid metals has led to much progress in the development of diffusion theories for liquid metals.

Theoretical models can be employed in predicting the values of self-diffusivities of pure liquid alloy components to a reasonable extent. One of such models was developed by Protopapas, Andersen and Parlee (1973). This is a model based on the hard-sphere theory and can be used to determine the self-diffusivities of liquid metals. According to Protopapas *et al*. (1973), the expression for self-diffusivities is given as:

$$D = \sigma C_{AW}(\eta)\left(\frac{\pi RT}{M}\right)^{1/2} \frac{(1-\eta)^3}{8\eta(2-\eta)} \ , \qquad (3.20)$$

where R is the universal gas constant, T is the temperature of investigation, M is the atomic weight, σ is the atomic diameter, η is the packing fraction and $C_{AW}(\eta)$ is known as the Alder-Wainwright correction.

An expression for the determination of σ is given as:

$$\sigma = 1.126\sigma_m[1 - 0.112(T/T_m)^{1/2}] \quad (3.21)$$

where σ_m is the atomic diameter at the melting temperature, T_m. By taking the melting-point packing fraction as $\eta_m = 0.472$ (Protopapas *et al.*, 1973), an expression for the computation of σ_m is given as:

$$\sigma_m = 1.41\left(\frac{M}{\pi\rho_m N_A}\right)^{1/3} \quad (3.22)$$

where ρ_m is the melting-point atomic density and N_A is Avogadro's constant.

The value of packing fraction at temperature T can be determined from the relation

$$\eta = \frac{0.472\ \rho\ \sigma^3}{\rho_m \sigma_m^3} \quad (3.23)$$

where in equation (3.23), ρ is the atomic density at a particular temperature T. An expression for the determination of ρ is given as:

$$\rho = \rho_m + \Lambda(T - T_m)\ , \quad (3.24)$$

where $\Lambda = \frac{\partial\rho}{\partial T}$

The value of Alder-Wainwright correction $C_{AW}(\eta)$ is required in equation (3.20). This value can be obtained from a chart in Protopapas *et al*. (1973) once the value of packing fraction η at any temperature of interest is known.

3.3.2 Viscosity

The concentration dependence of viscosity of binary liquid alloys shows linear relationship or positive or negative deviations from the linear law:

$$\xi_{id} = c\xi_A + (1 - c)\xi_B \quad (3.25)$$

The viscosity, ξ of a binary liquid alloy is given according to Moelwyn-Hughes (1961) as:

$$\xi = [c\xi_A + (1-c)\xi_B]\left[1 - 2c(1-c)\left(\frac{w}{KT}\right)\right], \quad (3.26)$$

where in equations (3.25) and (3.26), $\xi_i (i = A, B)$ are the viscosities of pure alloy components A and B respectively, w is the interchange energy and c is the concentration of atom A.

The temperature dependence of viscosity in liquid metals approximates an Arrhenius type expression (Iida & Guthrie, 1988). This is a relationship which can be employed in order to theoretically calculate the viscosity values of the alloy components at the working temperature (Anusionwu & Echendu, 2010). This is given as:

$$\xi = Q\ exp\left(\frac{H_\xi}{RT}\right), \quad (3.27)$$

where Q and H_ξ are constants.

The constant Q is given according to Grosse (1961) as:

$$Q = \frac{5.7\times10^{-2}(MT_m)^{1/2}}{\Omega_m^{2/3}\ exp(H_\xi/RT_m)}, \quad (3.28)$$

where in equations (3.27) and (3.28), M, R, T and Ω_m are the molecular weight, universal gas constant, temperature of investigation , and atomic volume at melting point, respectively.

In addition, Grosse (1961) showed that there is an empirical relationship between H_ξ for liquid metals and their melting temperatures, T_m. A similar work was carried

out by Iida, Morita and Takuchi (1975) and they gave the following expressions for H_ξ:

$$H_\xi = 1.21\, T_m^{1.2} \tag{3.29}$$

$$H_\xi = 0.75\, T_m^{1.2} \tag{3.30}$$

Equations (3.28) and (3.29) apply to normal metals and semi-metals respectively.

3.4 Surface properties

Prasad, Singh and Singh (1994) developed a statistical mechanical approach based on the concept of layered structure near the interface to obtain expressions for surface properties of binary liquid alloys. Based on this approach, the grand partition function at the surface, Ξ^S, surface tension, τ, and surface area Φ, are related through the expression given below:

$$\Xi^S = exp\left(\frac{-\tau\Phi}{KT}\right) = exp\left(\frac{-\tau\lambda N^S}{KT}\right), \tag{3.31}$$

where N^S, K and $\lambda\left(=\frac{\Phi}{N^S}\right)$ are the total number of atoms at the surface, Boltzmann constant, and mean atomic surface area respectively.

The surface tension of a binary liquid alloy can be determined through the activity coefficients of the alloy components. In terms of the activity coefficients of the alloy components, Prasad *et al.* (1994) gave two sets of equations for the calculation of surface tension of a binary liquid alloy as:

$$\tau = \tau_A + \frac{KT}{\lambda} ln \frac{C_A^S}{C_A} - \frac{KT}{\lambda} ln\, \gamma_A + \frac{w}{\lambda}[p(c_B^S)^2 + q(c_B)^2] \tag{3.32}$$

and

$$\tau = \tau_B + \frac{KT}{\lambda} ln \frac{C_B^S}{C_B} - \frac{KT}{\lambda} ln\, \gamma_B + \frac{w}{\lambda} [p(c_A^s)^2 + q(c_A)^2] \,, \qquad (3.33)$$

where τ_A and τ_B are the surface tension of pure alloy components A and B, c_i and c_i^s $(i = A, B)$ are the bulk and surface concentrations of the alloy components A and B, γ_A and γ_B are the bulk activity coefficients of the alloy components A and B and w is the interchange energy.

The ideal surface tension is given as:

$$\tau_{id} = \tau_A c_A + \tau_B c_B \qquad (3.34)$$

The surface $S_{cc}(0)$ is useful in studying how the atoms are arranged at the surface of an alloy. The surface $S_{cc}(0)$ is given according to Prasad and Singh (1991) as:

$$S_{cc}^s(0) = c_A^s\, c_B^s \left[1 + \left(\frac{Z^s}{2\beta^s}\right)(1 - \beta^s)\right]^{-1}, \qquad (3.35)$$

where

$$\beta^s = \left\{1 + 4\, c_A^s\, c_B^s \left[exp\left(\frac{w}{Z^s KT}\right) - 1\right]\right\}^{1/2} \qquad (3.36)$$

Here, Z is the coordination number in the bulk which is usually taken as 10 for most of liquid metallic systems (Prasad *et al.*, 1995). Z^s is the surface coordination number which is given as:

$$Z^s = Z(p + q) \,, \qquad (3.37)$$

where p and q are surface coordination fractions. p and q are fractions of total number of nearest neighbours an atom has within its own layer and that in the adjacent layer, respectively (Akinlade & Singh, 2002). The values of p and q are

chosen such that $p + 2q = 1$ (Prasad & Singh, 1991; Prasad *et al.*, 1998). For closed-packed structures, $p = 0.5$ and $q = 0.25$ (Anusionwu *et al.*, 2009).

The surface tension and atomic volume have temperature-dependent relationships which can be used to determine the surface tension and atomic volume of the alloy components at the temperature of investigation. These relationships are given in Smithells and Brandes (1978) as:

$$\tau_i = \tau_{im} + (T - T_m)\frac{\partial \tau_i}{\partial T} \tag{3.38}$$

and

$$\Omega_i = \Omega_{im}[1 + \theta(T - T_m)] \, , \tag{3.39}$$

where τ_{im} $(i = A, B)$ is the surafec tension of the alloy component i at the melting point, Ω_{im} $(i = A, B)$ is the atomic volume of the alloy component i at the melting temperature, T_m in Kelvin, θ is the thermal coefficient of expansion and $\frac{\partial \tau_i}{\partial T}$ $(i = A, B)$ is the temperature coefficient of surface tension.

Calculation of surface properties requires the mean surface area λ. According to Laty, Joud and Desre (1976), an expression for determining the atomic surface area λ_i for each component atom in binary liquid alloys is given as:

$$\lambda_i = 1.102\Omega_i^{2/3} N_A^{-2/3} \tag{3.40}$$

and the mean surface area λ is given as

$$\lambda = \sum c_i \lambda_i \, , \tag{3.41}$$

where N_A is the Avogadro's constant and $c_i (i = A, B)$ are the concentrations of the alloy components A and B respectively.

CHAPTER FOUR

RESULTS AND DISCUSSIONS

4.1 Results

The experimental values of Gibbs free energy of mixing and activities obtained from (Hultgren *et al.*, 1973) were used in conjunction with equations (3.3) and (3.6) to obtain optimised values of model parameters which give good overall representations of the experimental thermodynamic quantities of the alloys at all concentrations. The values of the model parameters obtained at 1863 K are shown in Table 4.1.

The model parameters shown in Table 4.1 were used to calculate the activity coefficients, concentration-concentration fluctuations at the long wavelength limit $S_{cc}(0)$, and Warren-Cowley chemical short-range order parameter (α_1). These quantities have been used in the determination of transport and surface properties.

Table 4.1: Model parameters for liquid Fe−Mn and Fe−Co alloys.

$Alloy$	Temperature $T\ (K)$	Ratio of self-associates (n)	Order energy parameter (W/RT)
Fe−Mn	1863	1.551	0.305
Fe−Co	1863	1.380	0.335

4.1.1 Thermodynamic properties

In figures 4.1 and 4.2 respectively, the calculated Gibbs free energy of mixing and activity values are compared with experimental values for liquid Fe−Mn alloy at 1863 K while in figures 4.3 and 4.4 respectively, the calculated Gibbs free energy of mixing and activity values are compared with experimental values for liquid Fe−Co alloy at 1863 K.

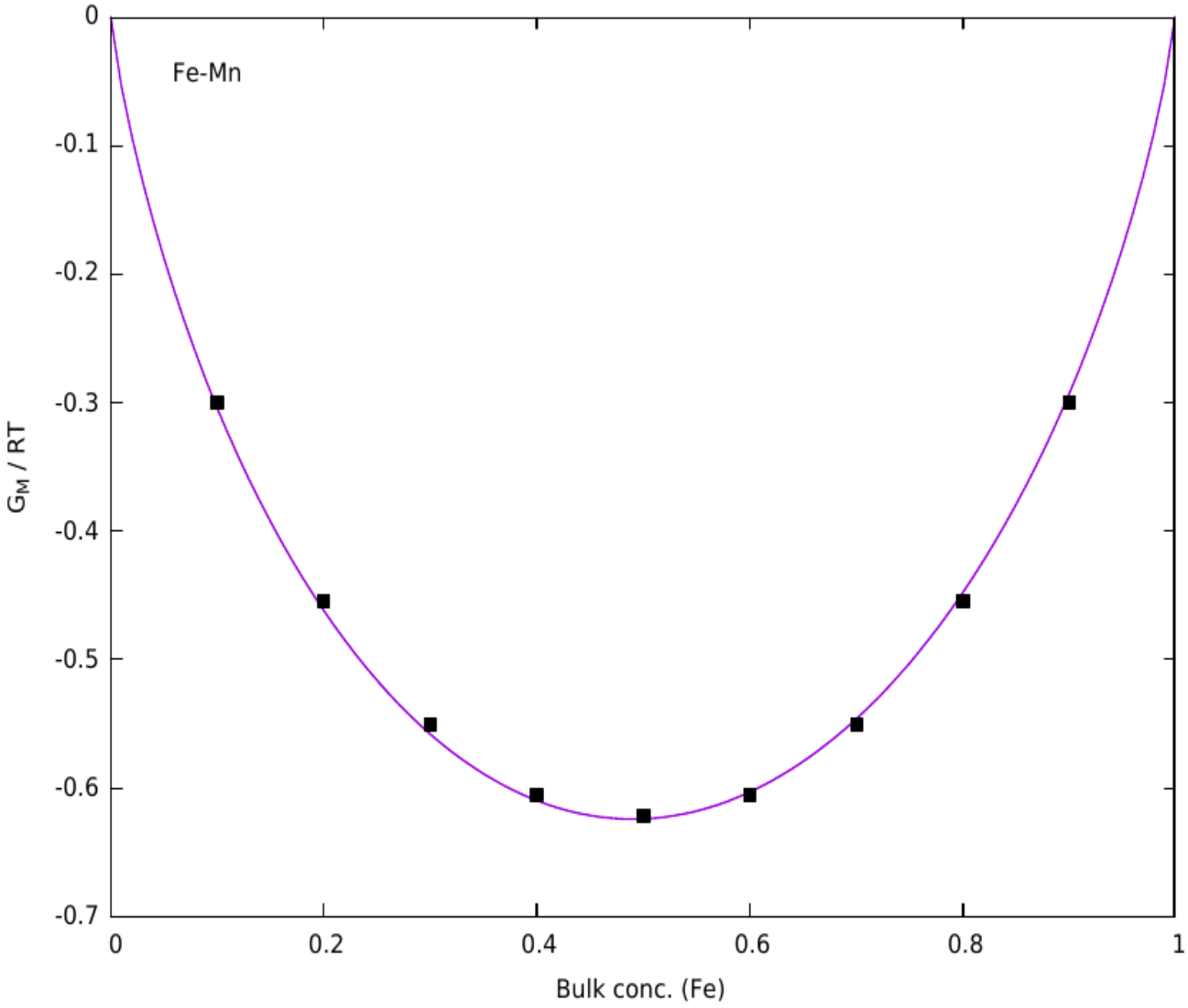

Figure 4.1: Calculated (line) and experimental (filled squares) values of G_M/RT against bulk concentration (Fe) for Fe−Mn alloy at 1863 K.

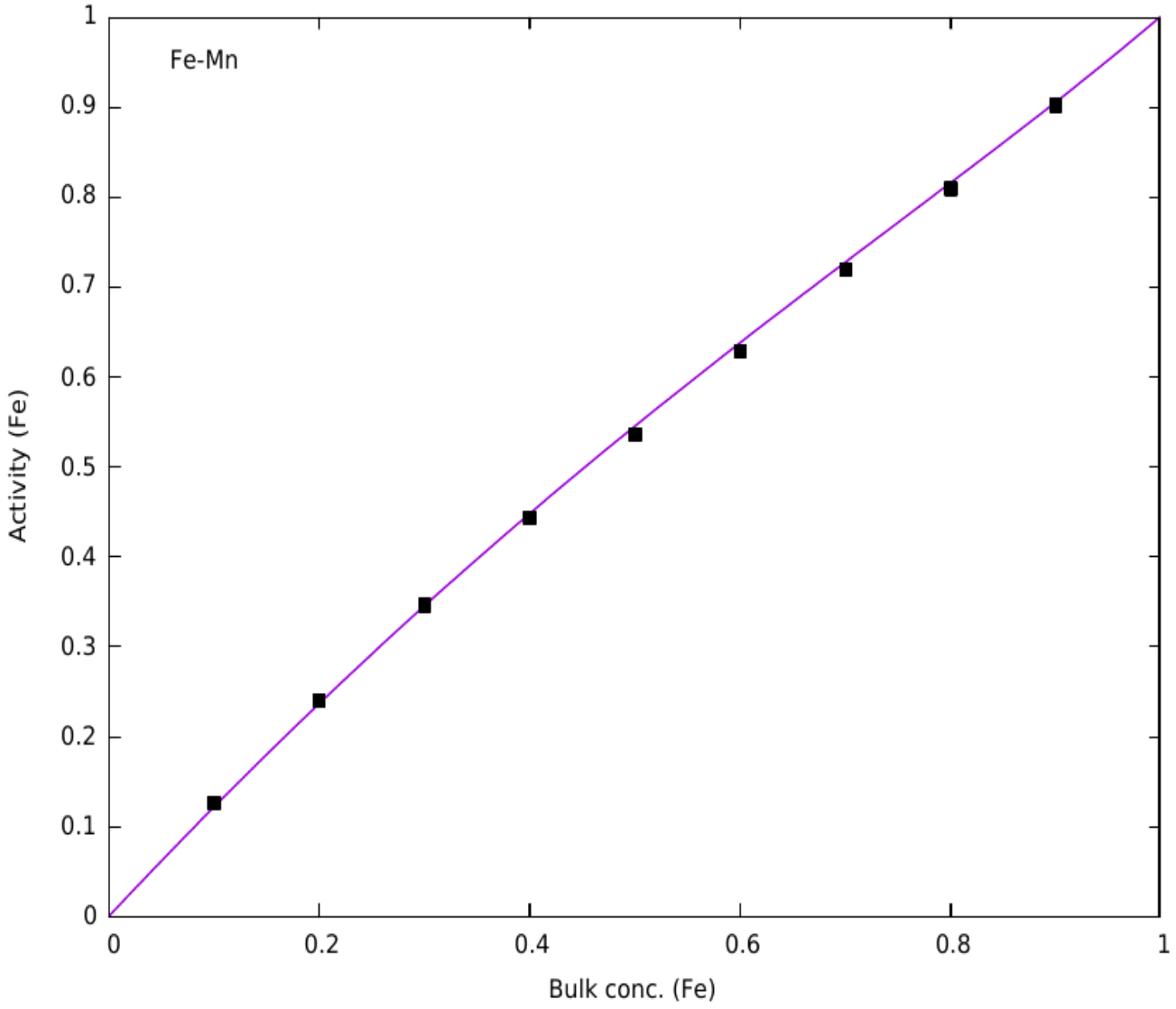

Figure 4.2: Calculated (line) and experimental (filled squares) of activity against bulk concentration (Fe) for Fe−Mn alloy at 1863 K.

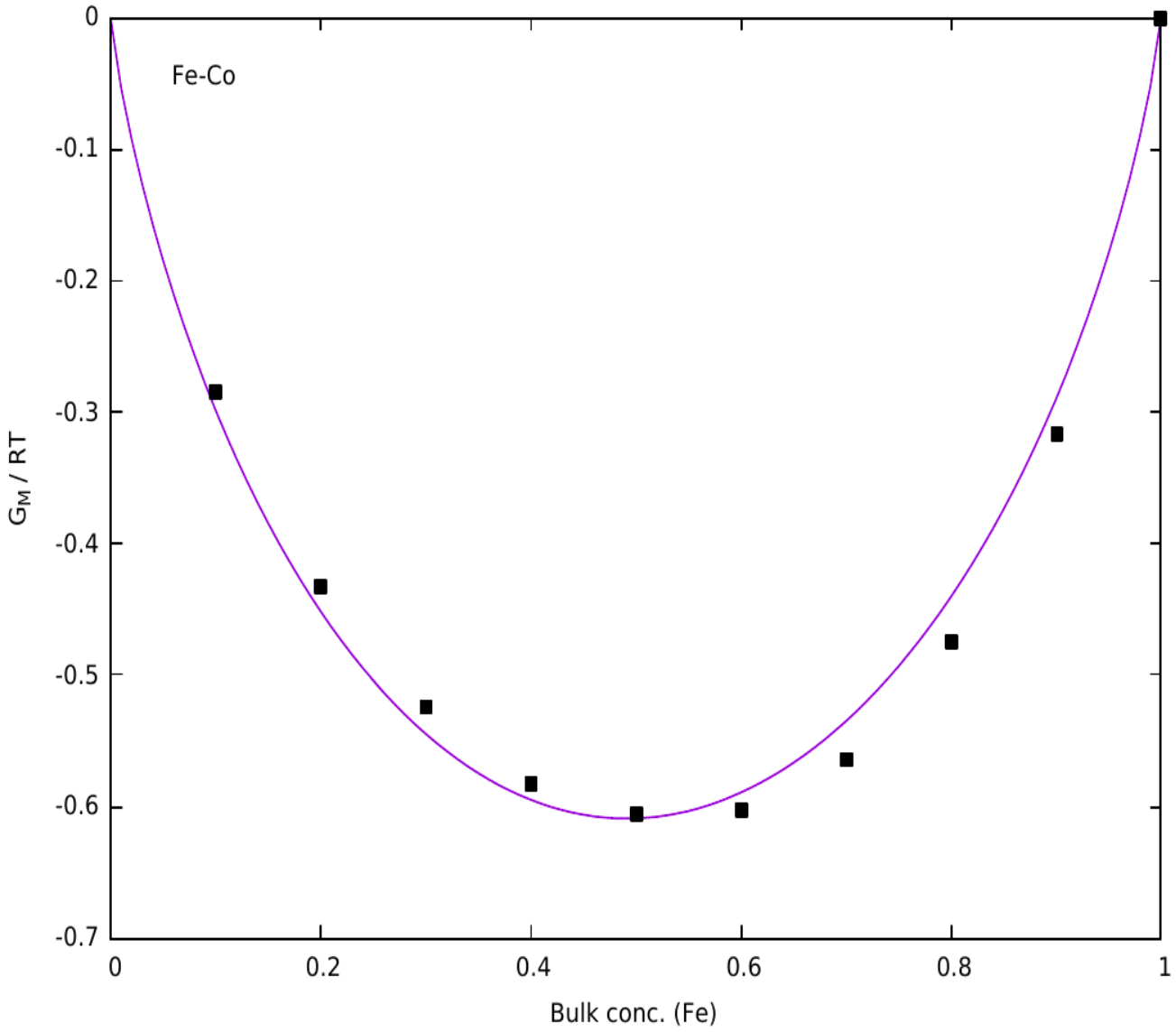

Figure 4.3: Calculated (line) and experimental (filled squares) values G_M/RT against bulk concentration (Fe) for Fe−Co alloy at 1863 K.

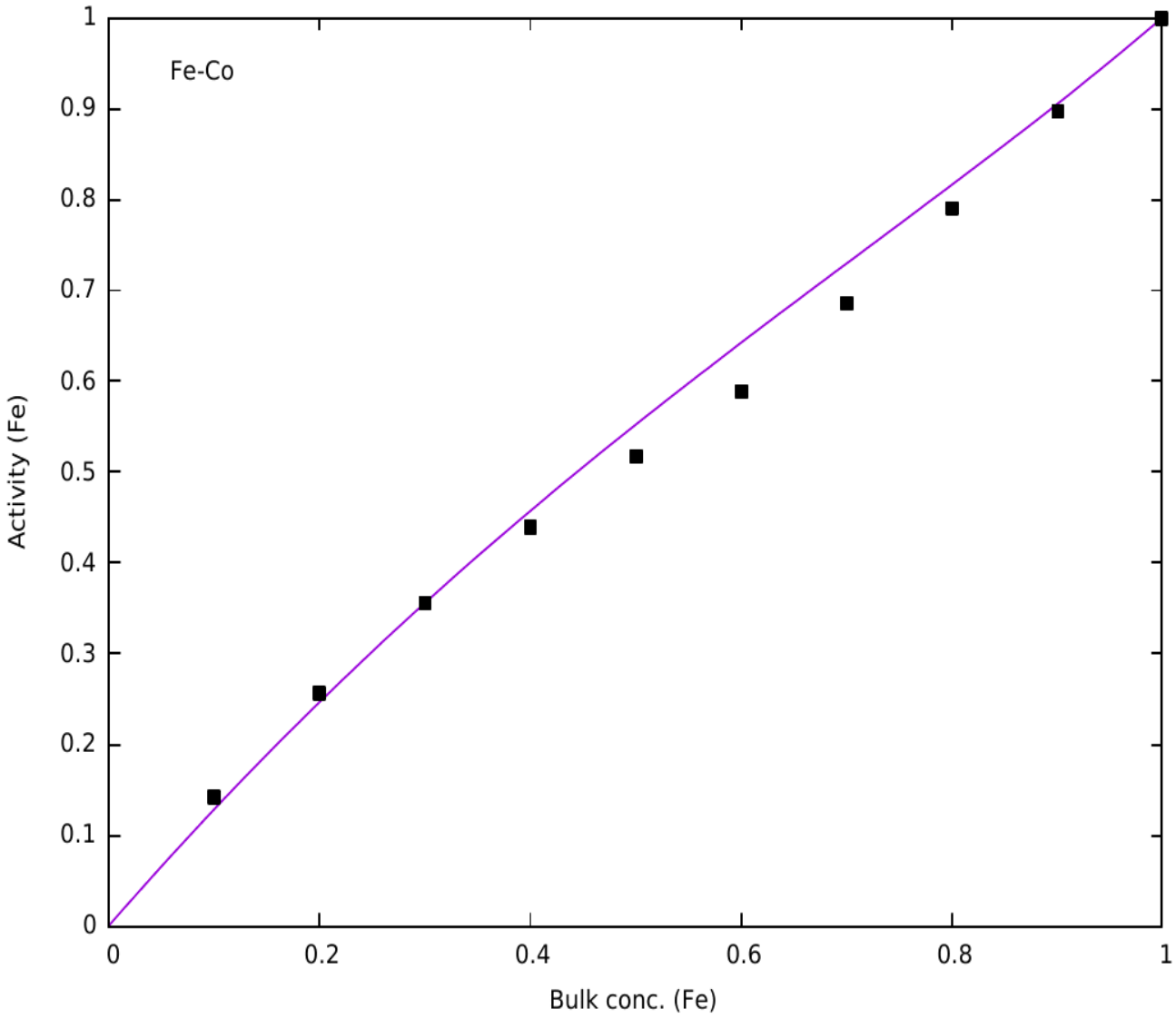

Figure 4.4: Calculated (line) and experimental (filled squares) values of activity against bulk concentration (Fe) for Fe−Co alloy at 1863 K.

4.1.2 Structural properties

Two functions which are usually made use of in order to study the local arrangement of atoms and the strength of interactions are concentration-concentration fluctuations at the long wavelength limit, $S_{cc}(0)$ and Warren-Cowley short range order parameter, α_1.

It has been reported that the extent of positive deviations of the concentration-concentration fluctuations at the long wavelength limit $S_{cc}(0)$ from its ideal values $S_{cc}^{id}(0)$ determines the strength of segregation in the bulk of the alloys (R N Singh & Sommer, 1997). In order to determine the strengths of segregation in the alloys at $1863\,K$, the concentration-concentration fluctuations at the long wavelength limit $S_{cc}(0)$, calculated from equation (3.10) using already determined model parameters was plotted as a function of bulk concentration. The experimental values of $S_{cc}(0)$ were determined from measured activity values using equation (3.9) and compared with the calculated values.

Figure 4.5 shows the variation of $S_{cc}(0)$ with the bulk concentration of iron (Fe) for liquid Fe−Mn while figure 4.6 shows the variation of $S_{cc}(0)$ with the bulk concentration of iron (Fe) for liquid Fe−Co alloys.

There is a slight deviation between the calculated and the ideal values of $S_{cc}(0)$ for liquid Fe−Mn alloy as shown in figure 4.5. The $S_{cc}(0)$ is symmetric around the equiatomic concentration. The extent of homocoordination in this alloy is low.

The calculated and experimental values of $S_{cc}(0)$ are not in agreement for liquid Fe−Co alloy as shown in figure 4.6. Experimental $S_{cc}(0)$ shows asymmetry while the calculated $S_{cc}(0)$ is symmetric around the equiatomic concentration. . It is observed that the model of Singh and Sommer (1992) for regular alloys could not reproduce quantitatively the experimental values of $S_{cc}(0)$ for liquid Fe−Co alloy.

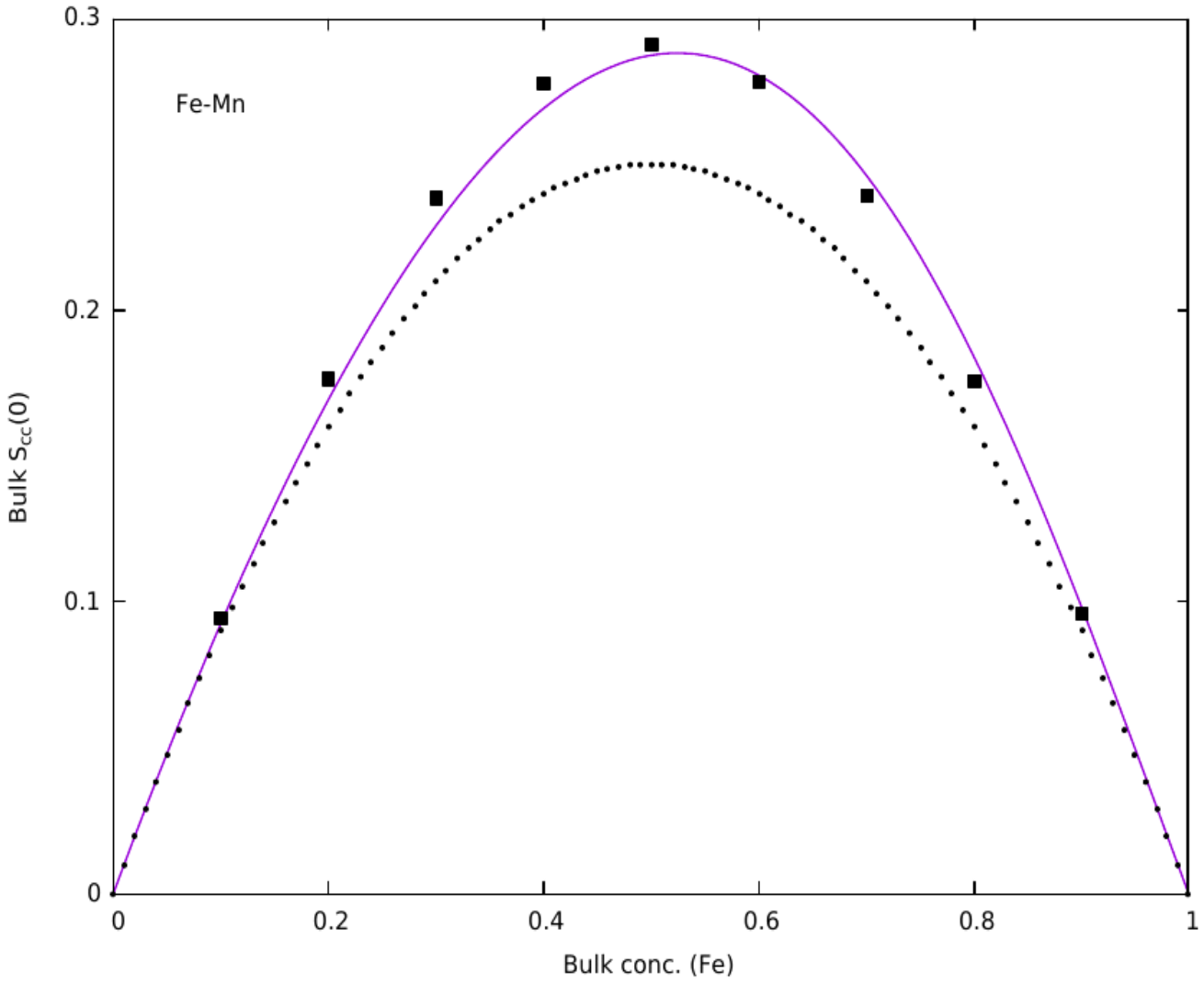

Figure 4.5: Bulk $S_{cc}(0)$ against bulk concentration (Fe) for Fe−Mn alloy at 1863 K. Line and filled squares are calculated and experimental values of $S_{cc}(0)$, respectively. Dots represent the ideal $S_{cc}(0)$.

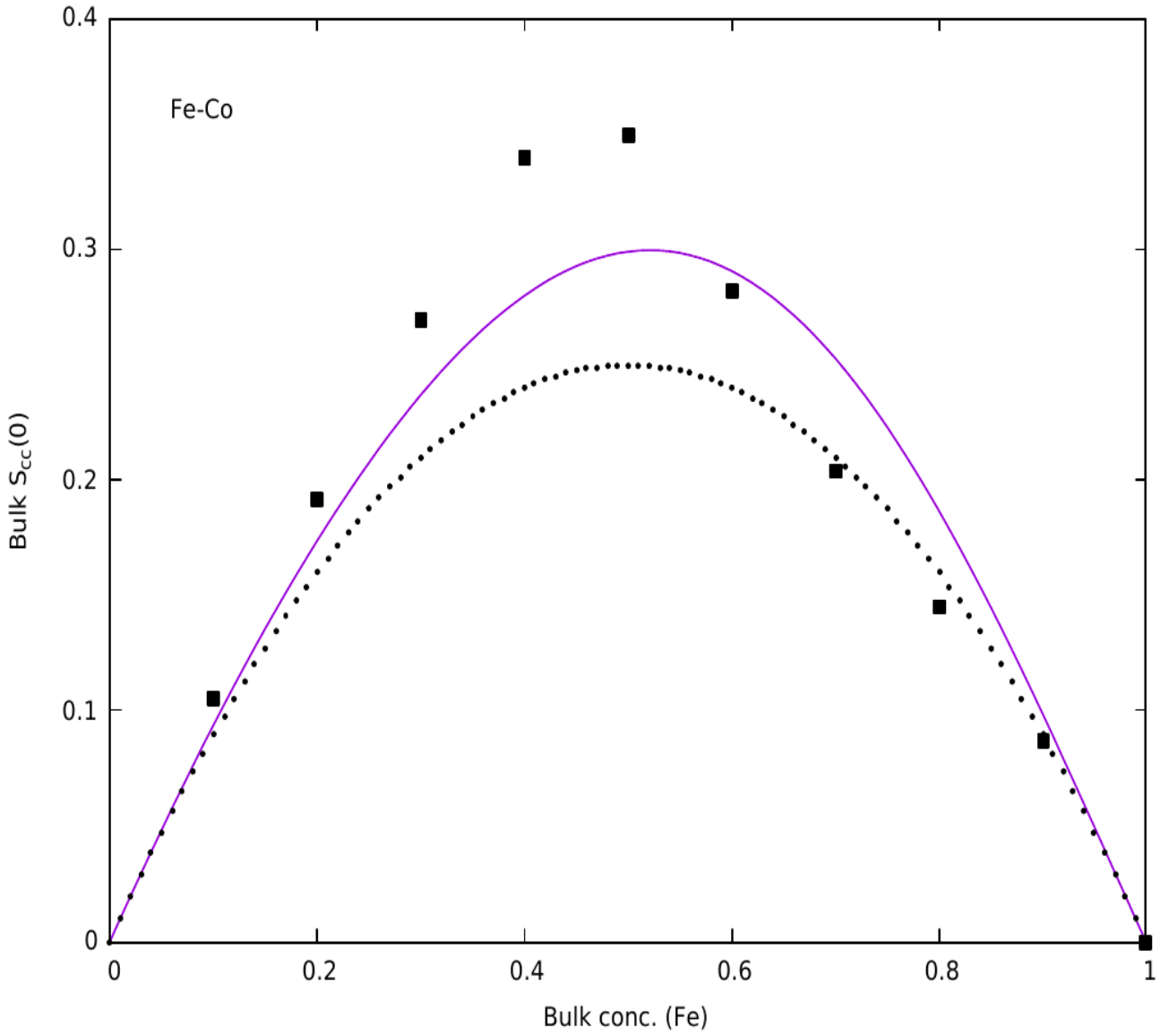

Figure 4.6: Bulk $S_{cc}(0)$ against bulk concentration (Fe) for Fe−Co alloy at 1863 K. Line and filled squares are calculated and experimental values of $S_{cc}(0)$, respectively. Dots represent the ideal $S_{cc}(0)$.

The short-range order parameter, α_1 calculated from equation (3.16) was also plotted against bulk concentration of iron (Fe) to shed light on the ordering phenomena in Fe−Mn and Fe−Co alloys. Figure 4.7 shows the plot of α_1 against the bulk concentration of iron (Fe) for Fe−Mn and Fe−Co alloys. Figure 4.7 shows that the degree of phase segregation is higher in Fe−Co alloy than in Fe−Mn alloy.

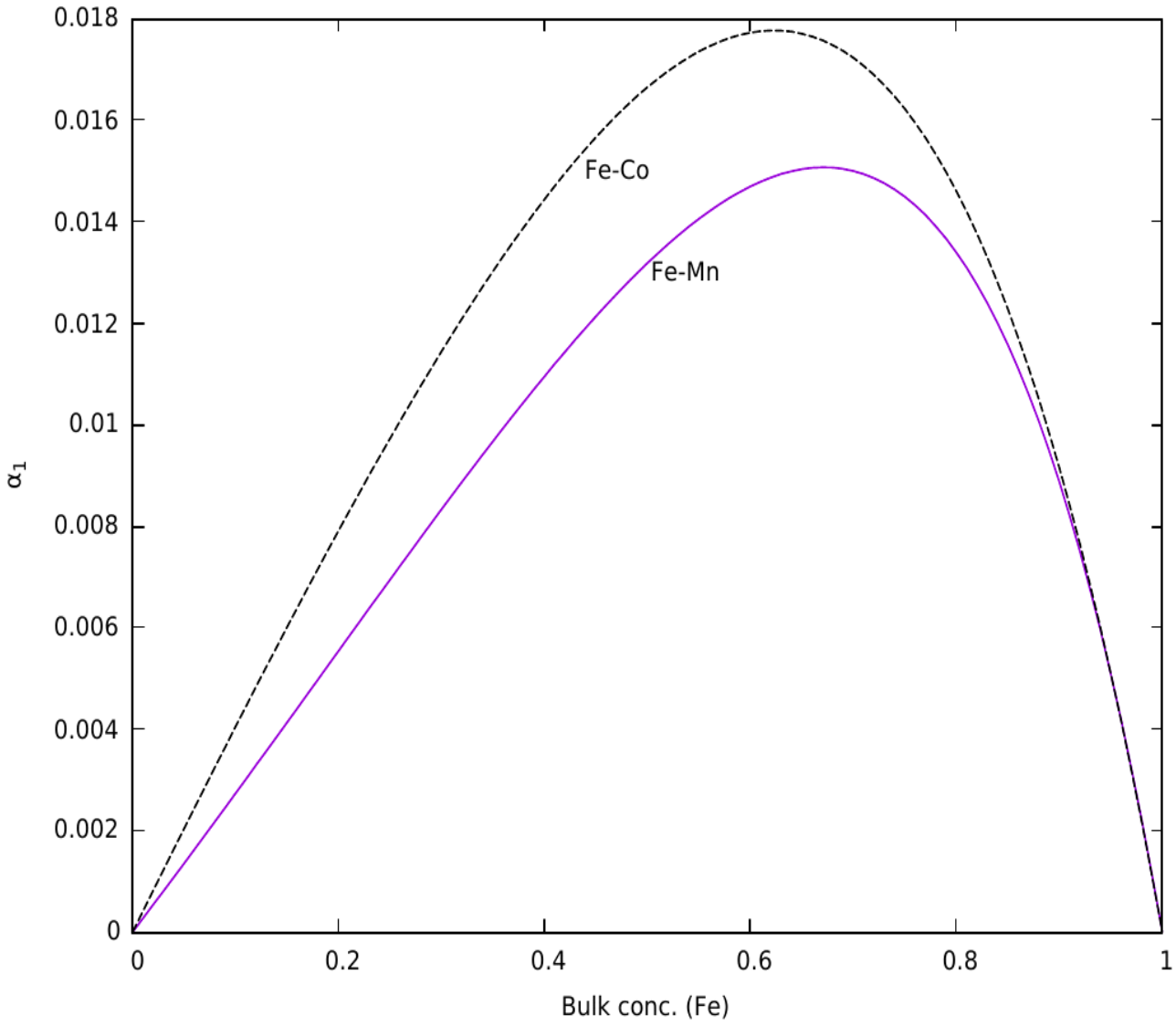

Figure 4.7: α_1 against bulk concentration of iron (Fe) for Fe−Mn and Fe−Co alloys at 1863 K.

4.1.3 Transport properties

Using equation (3.18), the mutual diffusivity D_M for the two liquid alloys were calculated at $1863\ K$. To calculate the values of mutual diffusivity, the values of self-diffusivities of pure Fe, Mn and Co at 1863K are required. Due to unavailability of experimental values of self-diffusivities for Fe, Mn and Co at $1863\ K$, the model of Protopapas *et al*. (1973) given in equation (3.20) was used to calculate the values of self-diffusivities for the components of Fe−Mn and Fe−Co alloys. Experimental and calculated values of self-diffusivities of some liquid metals at their melting points are compared in Table 4.2.

The experimental values of self-diffusivities at the melting points of Ga, Ag and K were obtained from Protopapas *et al*. (1973) while the value for Fe was obtained from Yokoyama (1999).

The calculated values for these liquid metals are in close agreement with experimental values. Thus, the model was used to determine the values of self-diffusivities for Fe, Mn and Co at $1863\ K$. The values of M, ρ_m and Λ in equations (3.20), (3.22)−(3.24) were taken from Iida & Guthrie (1988). After determining the packing fraction, η at 1863 K for the alloy components, the value of Alder-Wainwright correction factor, $C_{AW}(\eta)$ was obtained from a chart in Protopapas *et al*. (1973). The self-diffusivities obtained at 1863 K for Fe, Mn and Co are 4.18, 7.97 and 4.49 ($\times 10^{-9} m^2 s^{-1}$) respectively.

Table 4.2: Comparison of calculated melting-point self-diffusivities of some liquid metals from equation (3.20) with experimental values.

Metals	Calculated self-diffusivity $(10^{-9}\ m^2 s^{-1})$	Experimental self-diffusivity $(10^{-9}\ m^2 s^{-1})$
Fe	4.07	4.16
Ga	1.69	1.72
Ag	2.75	2.55
K	3.81	3.82

Figures 4.8 and 4.9 show the variation of mutual diffusivity with bulk concentration of iron (Fe) for the liquid Fe−Mn and Fe−Co alloys respectively. For Fe−Mn alloy, the mutual diffusivity decreases almost like for a regular alloy to around 0.85 atomic fraction of iron (Fe) as shown in figure 4.8. For the Fe−Co alloy, the mutual diffusivity shows a negative departure from ideality. The two plots show that diffusion-related activities will be higher in liquid Fe−Mn alloy than in liquid Fe−Co alloy.

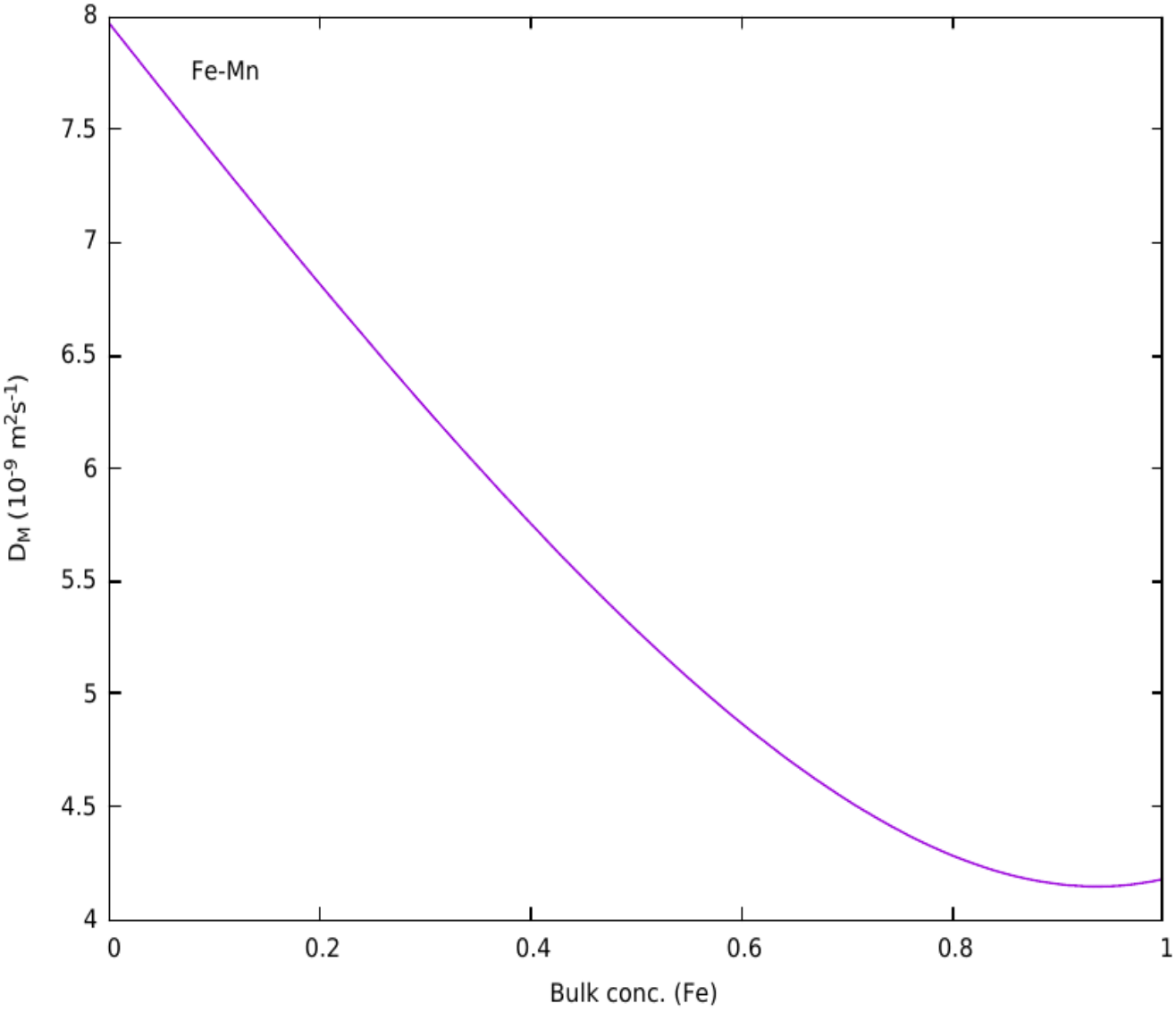

Figure 4.8: Mutual diffusivity against bulk concentration (Fe) for Fe−Mn alloy at $1863\ K$.

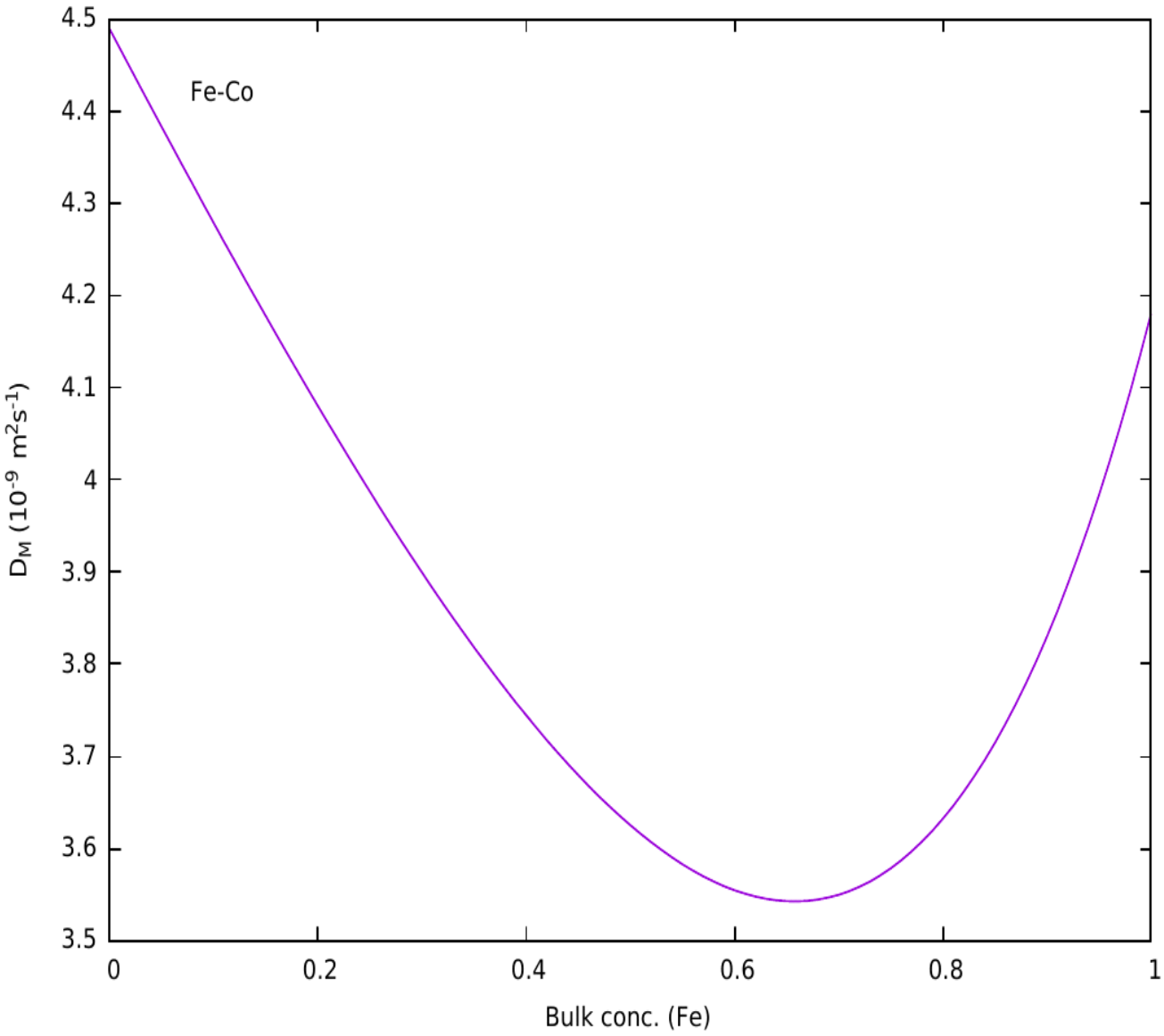

Figure 4.9: Mutual diffusivity against bulk concentration (Fe) for Fe−Co alloy at 1863 K.

The viscosities of the two liquid alloys were computed from the model of Moelwyn-Hughes (1961) given in equation (3.26). To do this, the values of viscosity of pure Fe, Mn and Co at $1863\ K$ are required. Due to lack of experimental viscosity values of the alloy components at 1863 K, equation (3.27) was used to predict their viscosities at this temperature. Table 4.3 shows the comparison of experimental viscosity values of Fe, Mn and Co with calculated values using Arrhenius type equation (3.26).

The experimental values of viscosity for Fe, Mn and Co were obtained from Kaptay (2005). The calculated values of viscosity for these liquid metals at their melting points are in close agreement with experimental values. Thus, equation (3.27) was used to predict the values of viscosity for Fe, Mn and Co at $1863\ K$. The calculated values of viscosities of Fe, Mn and Co were substituted into equation (3.26) to determine the viscosities of Fe−Mn and Fe−Co alloys throughout the whole concentration range.

Table 4.3: Viscosity values of some liquid metals. Calculated values were obtained using Arrhenius type equation (3.27).

Metals	Experimental viscosity at melting point ($mPas$)	Calculated viscosity at melting point ($mPas$)	Calculated viscosity at 1863 K ($mPas$)
Fe	4.1 – 5.3	4.55	4.46
Mn	5.0	3.66	3.25
Co	4.7 – 6.2	4.76	4.60

Figures 4.10 and 4.11 show the variation of viscosity with bulk concentration of iron (Fe) for liquid Fe−Mn and Fe−Co alloys respectively. For the liquid Fe−Mn alloy, there is a small negative deviation from the linear law in viscosity as observed in figure 4.10. On the other hand, for liquid Fe−Co alloy there is a large negative deviation from the linear law in viscosity of about 0.83 $mPas$ as seen in figure 4.11.

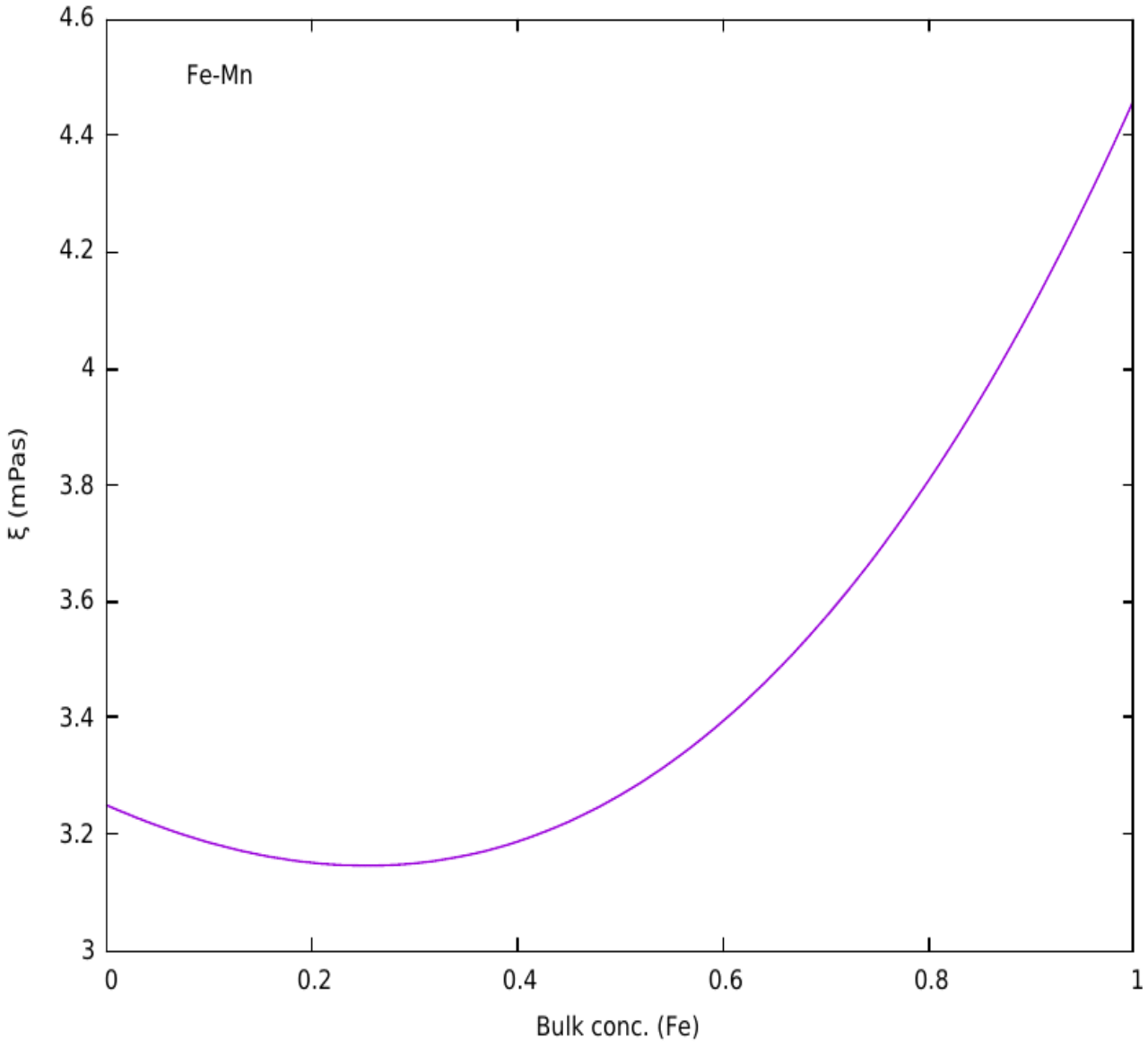

Figure 4.10: Viscosity against bulk concentration (Fe) for Fe−Mn alloy at 1863 K.

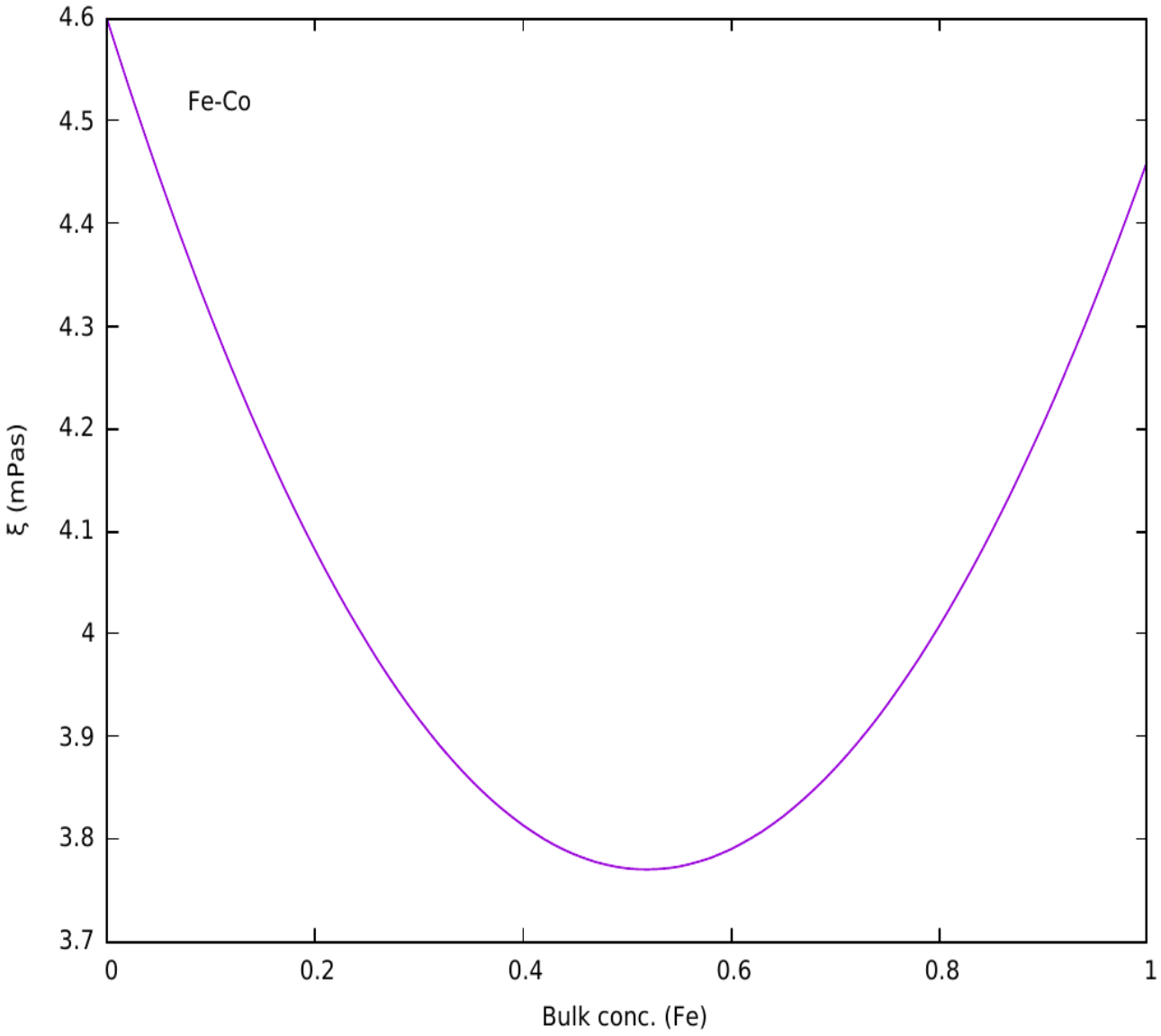

Figure 4.11: Viscosity against bulk concentration (Fe) for Fe−Co alloy at 1863 K.

4.1.4 Surface properties

The values of surface properties (surface concentrations and surface tension) of liquid Fe−Mn and Fe−Co alloys were computed numerically from equations (3.32) and (3.33). The two equations were solved simultaneously. The activity coefficients for Fe, Mn and Co atoms in liquid Fe−Mn and Fe−Co alloys, respectively, at $1863\ K$ were computed from equation (3.8) through equations (3.6) and (3.7) using the model parameters shown in Table 4.1.

The surface tension and atomic volume of Fe, Mn and Co at their melting temperatures were taken from Iida and Guthrie (1988). In order to obtain the surface tension and atomic volume at $1863\ K$ for the components of both liquid alloys, equations (3.38) and (3.39) were used. The values of $\frac{\partial \tau_i}{\partial T}$ and θ for pure Fe, Mn and Co were taken from Iida and Guthrie (1988). Equations (3.40) and (3.41) were used respectively to calculate the atomic surface area λ_i and the mean surface area λ for Fe, Mn and Co.

The surface tension values obtained at $1863\ K$ for Fe, Mn and Co are 1.845, 1.020 and 1.825 (Nm^{-1}) respectively. For atomic volume at $1863\ K$, the values are 8.00, 10.10 and 7.70 $(\times\ 10^{-6} m^3 mol^{-1})$ for Fe, Mn and Co respectively.

Figure 4.12 shows the variation of surface concentration of iron (Fe) with its bulk concentration for liquid Fe−Mn alloy while figure 4.13 shows the variation of surface concentration of iron (Fe) with its bulk concentration for liquid and Fe−Co alloy. For the liquid Fe−Mn alloys, figure 4.12 shows a negative deviation from

ideality. From figure 4.13, the surface concentration of liquid Fe−Co alloys is close to ideality. The presence of more iron (Fe) atoms at the surface of Fe−Co alloy suggests that Fe−Mn alloy will be more resistant to corrosion than Fe−Co alloy.

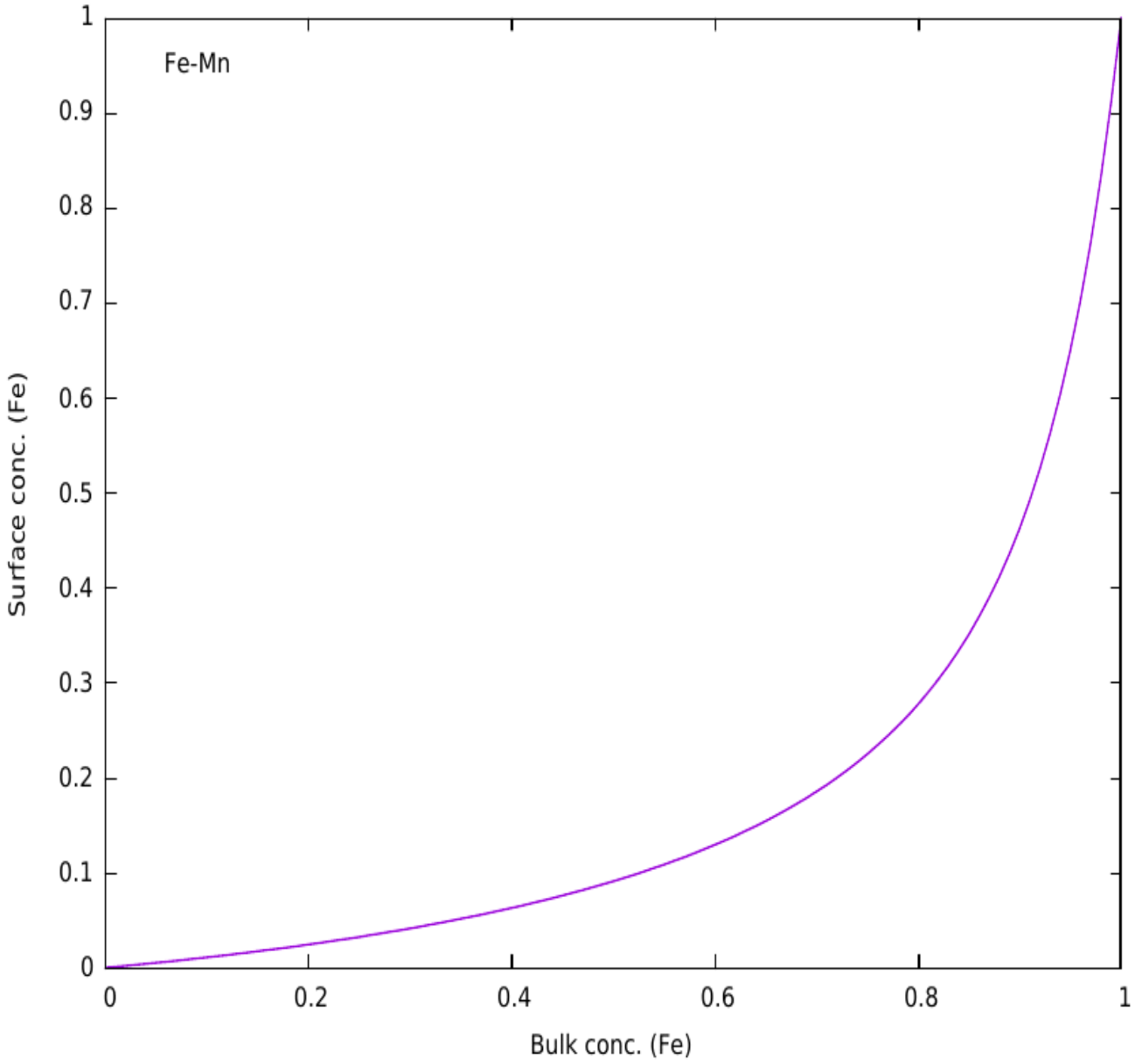

Figure 4.12: Surface concentration (Fe) against bulk concentration (Fe) for Fe−Mn alloy at 1863 K.

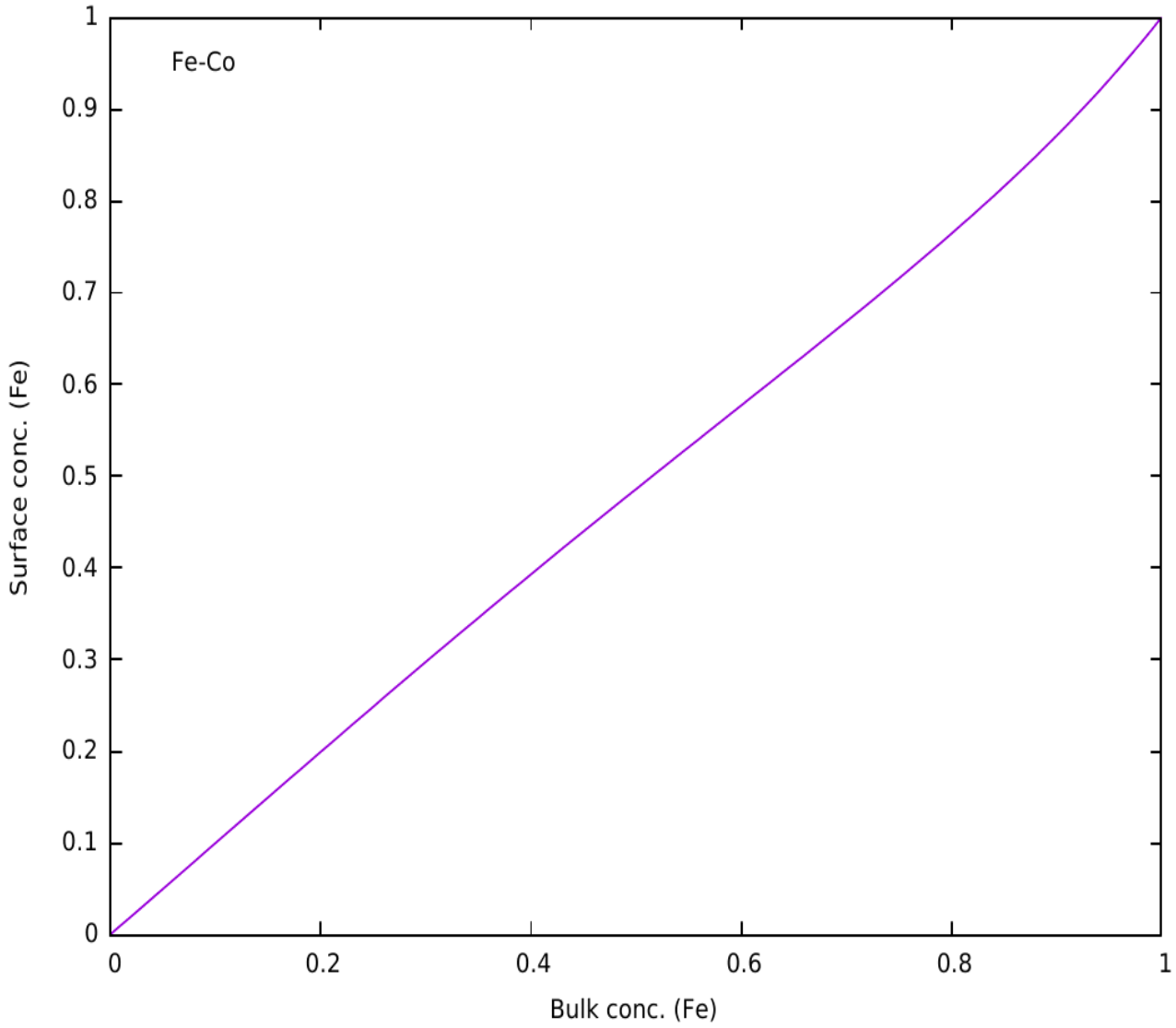

Figure 4.13: Surface concentration (Fe) against bulk concentration (Fe) for Fe−Co alloy at 1863 K.

Figures 4.14 and 4.15 show the plots of calculated surface tension values against bulk concentration of iron (Fe) for Fe−Mn and Fe−Co alloys respectively. For lack of experimental data at 1863 K, the calculated surface tension values for both liquid alloys could not be compared with experiment. However, calculations based on this model had shown close agreement with experiment (Anusionwu, Akinlade, & Hussain, 1998). The surface tension of Fe−Mn and Fe−Co alloys indicate a negative deviation from ideality.

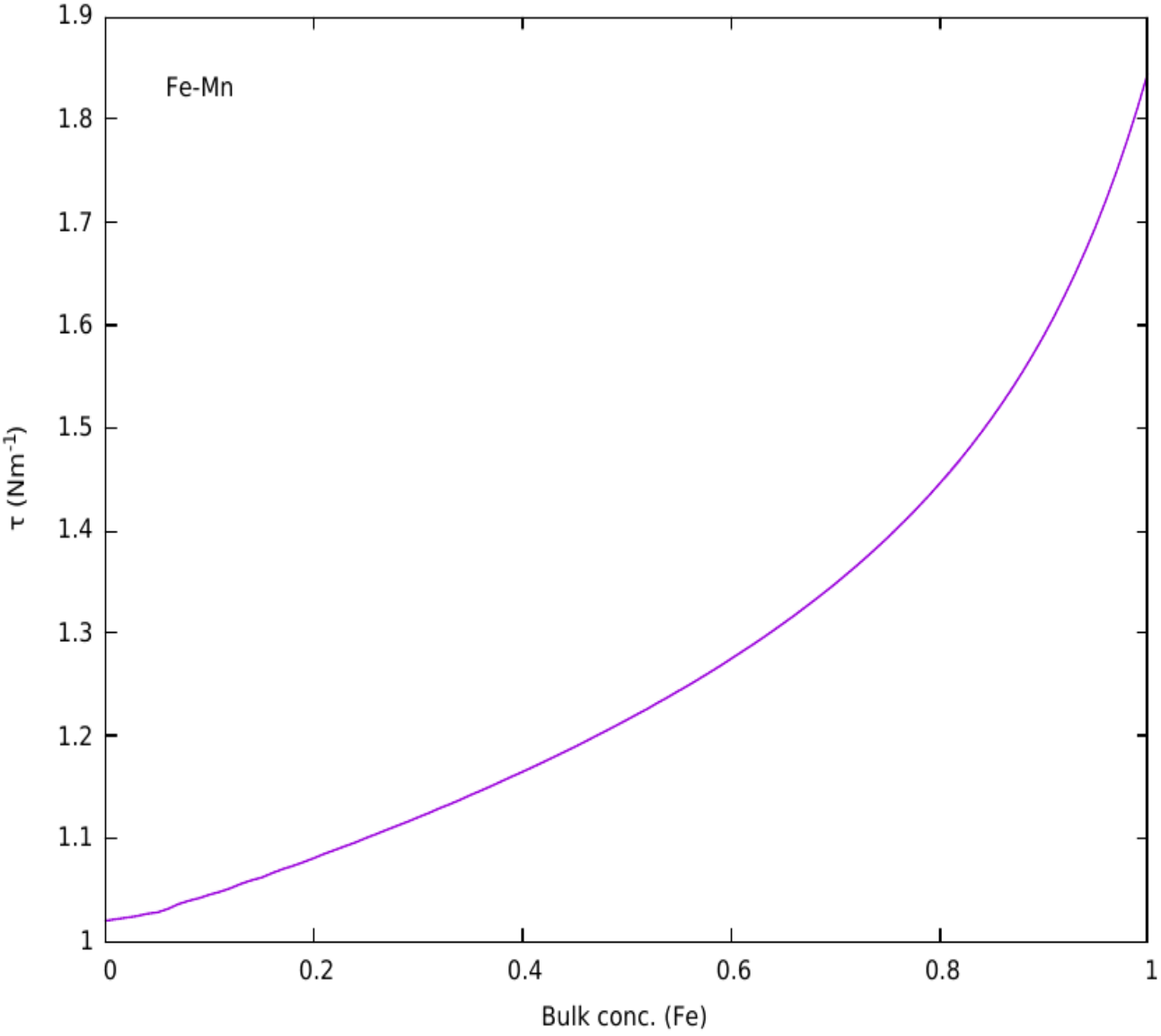

Figure 4.14: Surface tension against bulk concentration (Fe) for Fe−Mn alloy at 1863 K.

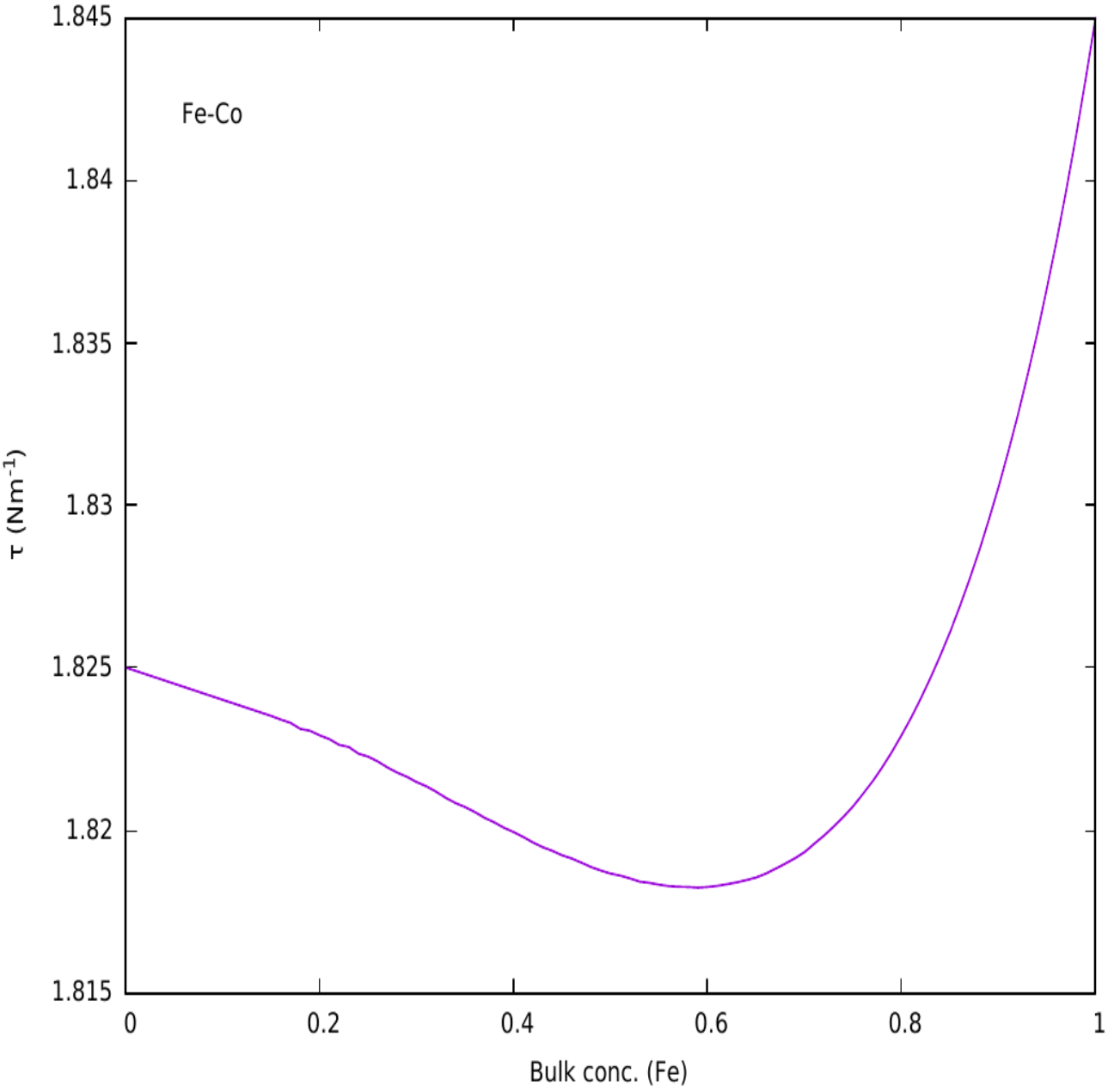

Figure 4.15: Surface tension against bulk concentration Fe) for Fe−Co alloy at 1863 K.

Surface $S_{cc}(0)$ gives the local arrangement of atoms at the surface of liquid alloys. Figures 4.16 and 4.17 show the variation of surface $S_{cc}(0)$ with bulk concentration of iron (Fe) for liquid Fe−Mn and Fe−Co alloys respectively. Fe−Mn alloy exhibits ideal behaviour below 0.4 and above 0.95 atomic fractions of iron at the surface. On the other hand, Fe−Co alloy exhibits ideal behaviour below 0.12 and above 0.9 atomic fraction of irons. These corroborate the results from bulk properties calculations.

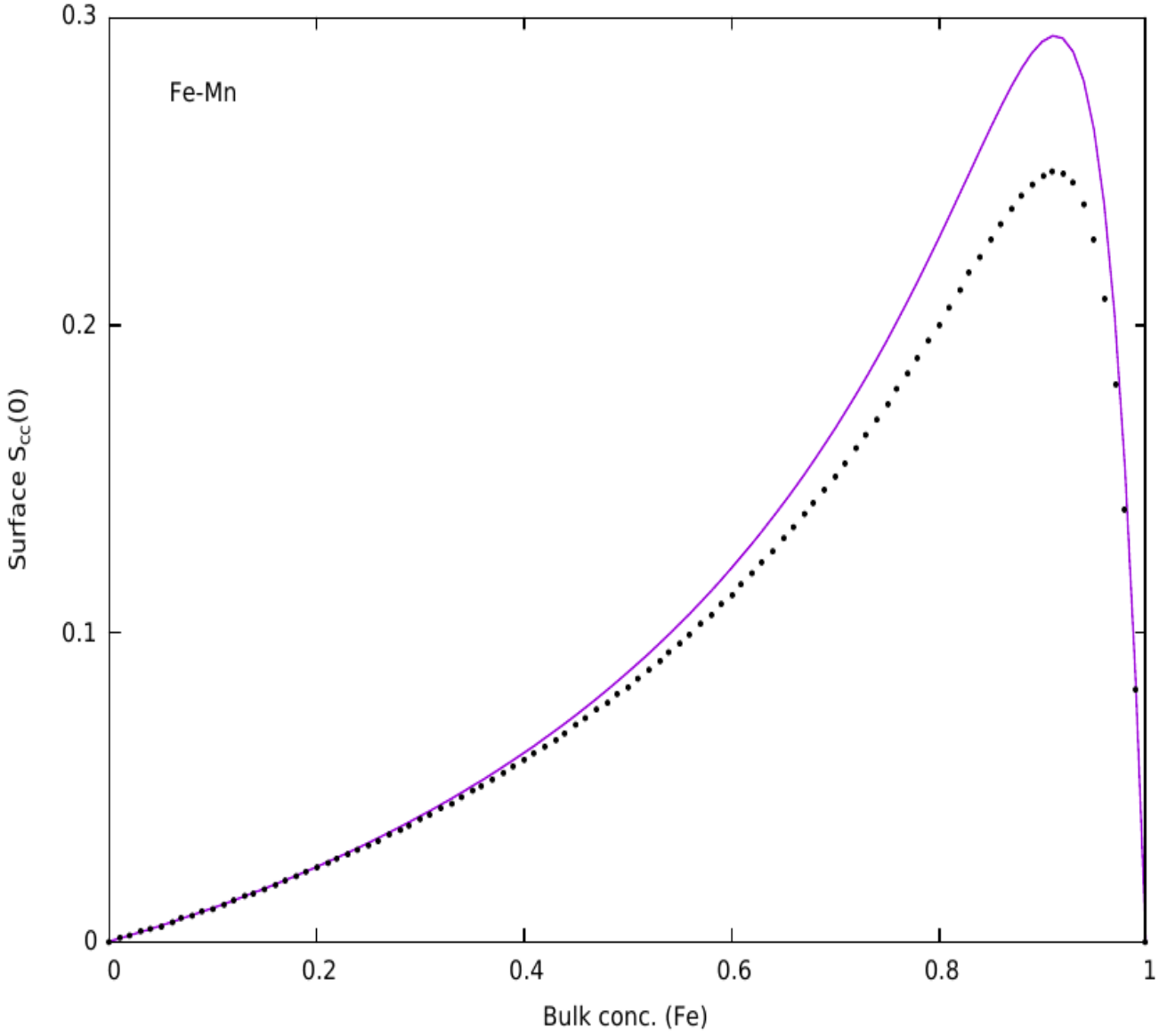

Figure 4.16: Surface $S_{cc}(0)$ against bulk concentration (Fe) for Fe−Mn alloy at 1863 K. Dots represent ideal values.

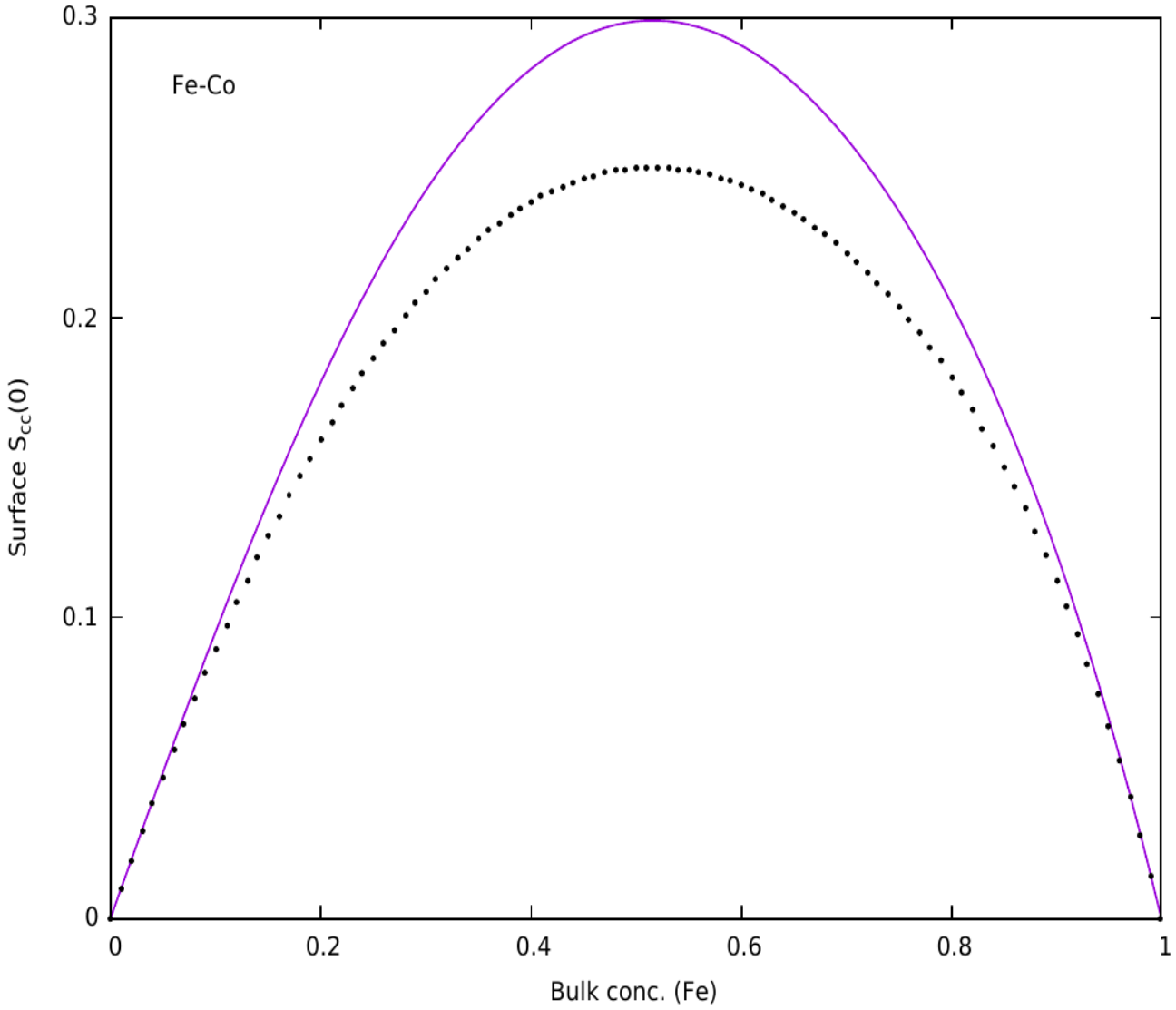

Figure 4.17: Surface $S_{cc}(0)$ against bulk concentration (Fe) for Fe−Mn alloy at 1863 K. Dots represent ideal values.

4.2 Discussions

Thermodynamic properties calculations show that for liquid Fe−Mn alloy, the calculated and the experimental values for Gibbs free energy of mixing at 1863 K are in excellent agreement (Fig. 4.1). It is also observed that the Gibbs free energy of mixing is symmetric around the equiatomic concentration. Similarly, the calculated and the experimental values of activity at 1863 K are in excellent agreement (Fig. 4.2). The activity values appear to obey Raoult's law. These observations suggest that liquid Fe−Mn alloy exhibits properties of ideal mixing with no tendencies to form complexes.

It is observed that for liquid Fe−Co alloy, there is some level of qualitative agreement between its calculated and the experimental Gibbs free energy of mixing at 1863 K (Fig. 4.3) . The experimental values of the Gibbs free energy of mixing have some slight asymmetry about equiatomic concentration which the calculated values could not reproduce quantitatively. For activity, there is also some level of qualitative agreement between the calculated and experimental values (Fig. 4.4). Also, the calculated and experimental values of activity show some disparity between 0.5 and 0.9 atomic fractions of iron (Fe). These observations suggest that, unlike Fe−Mn, liquid Fe−Co alloy do not exhibit properties of a regular alloy. This possibly suggests the presence of some complex forming activities in the liquid alloy at the temperature of investigation. However, no complexes were suggested in the phase diagram of Fe−Co alloy (Hultgren *et al*., 1973); therefore the self-association model was used to study the alloy.

Fe−Mn alloy exhibits ideal mixing property below 0.25 and above 0.88 atomic fractions of iron while in the rest of the concentration of iron, it shows low tendency for homocoordination. Hence the alloy has a regular behaviour with more tendency to ideal mixing where $S_{cc}(0) \cong S_{cc}^{id}(0)$ at all concentrations. Liquid Fe−Co alloy exhibits ideal mixing property below 0.20 and above 0.88 atomic fractions of iron while it shows tendency for homocoordination between 0.2 and 0.7 atomic fractions of iron. The experimental $S_{cc}(0)$ appear to be slightly below the ideal values between 0.70 and 0.90 atomic fractions of iron (Fe). This possibly suggests that at these concentrations, weak ordering is expected in the alloy.

Small positive values of α_1 clearly indicate that the two systems are weakly segregating (Fig. 4.7). Maximum segregation will occur around 0.67 atomic fraction of Fe for Fe−Mn alloy with the maximum value of $\alpha_1 \approx 0.0151$. For Fe−Co alloy, maximum segregation will occur around 0.62 atomic fraction of Fe with the maximum value of $\alpha_1 \approx 0.0178$.

On transport properties, above 0.85 atomic fraction of iron (Fe), the mutual diffusivity of Fe−Mn alloy remains almost constant (Fig. 4.8). Within this region diffusion-related activities will be low in the alloy. For Fe−Co alloy, there is a decrease in mutual diffusivity with increasing bulk concentration of iron (Fe) with the minimum value lying between 0.65 and 0.70 atomic fractions of iron (Fe) (Fig. 4.9). Around these concentrations, some complex forming activities are suspected. These activities must have led to a significant decrease in diffusion-related activities in this region in the alloy. The two plots show that diffusion-related activities will be higher in liquid Fe−Mn alloy than in liquid Fe−Co alloy.

Viscosity calculation shows that for the liquid Fe−Mn alloy, there is a small negative deviation from the linear law in viscosity (Fig. 4.10). Around 0.25 atomic fraction of iron (Fe), the viscosity is observed to decrease slightly by about 0.10 $mPas$ and then rises rapidly above this concentration. On the other hand, for liquid Fe−Co alloy there is a large negative deviation from the linear law in viscosity of about 0.83 $mPas$ (Fig. 4.11). The viscosity decreases rapidly to around 0.52 atomic fraction of iron (Fe) and then rises rapidly above this concentration. The minimum viscosity is expected between 0.50 and 0.57 atomic fractions of iron (Fe).

The surface concentration of Fe−Mn alloy shows that manganese with lower surface tension with respect to iron has more concentration at the surface (Fig. 4.12). On the other hand, iron atoms having higher value of surface tension remain in the bulk. This suggests that alloys of Fe and Mn are likely to be less susceptible to corrosion. Both Fe and Co atoms have almost equal concentrations at the surface of Fe−Co alloys (Fig. 4.13).

The surface tension of liquid Fe−Mn alloy increases with increasing bulk concentration of iron (Fig. 4.14). On the other hand, the surface tension of liquid Fe−Co alloy decreases with increase in the bulk concentration of iron to around 0.59 atomic fraction of iron (Fe) and then rises rapidly (Fig. 4.15). Reduction of surface tension in Fe−Co alloy to above the equiatomic concentration may be as a result of the suspected complex forming activities within this region. The extent of surface segregation may not be significant in the two alloys (Fig. 4.16 and Fig. 4.17)

CHAPTER FIVE

CONCLUSION AND RECOMMENDATION

5.1 Conclusion

The self-association model of Singh and Sommer (1992) has been used in conjunction with a model based on the hard-sphere theory, the model of Moelwyn-Hughes and a statistical mechanical approach to compute the transport and surface properties of liquid Fe−Mn and Fe−Co alloys. Calculations indicate that both alloys are weak phase segregating systems. While Fe−Mn alloy tends towards ideal mixing of a regular alloy, Fe−Co alloy shows ideal mixing property below 0.20 and above 0.88 atomic fractions of iron (Fe), homocoordination between 0.20 and 0.70 atomic fractions of iron (Fe) and weak ordering between 0.7 and 0.9 atomic fractions of iron (Fe).

Calculations of transport properties show that the mutual diffusivity of Fe−Mn alloy decreases with increasing bulk concentration of iron (Fe) to around 0.85 atomic fraction of iron (Fe) and remains almost constant. However, for Fe−Co alloy, the mutual diffusivity shows a negative departure from ideality with the minimum value lying between 0.65 and 0.70 atomic fractions of iron (Fe). Within the regions of low mutual diffusivities in the two systems, diffusion-related activities will be relatively low. The plots of mutual diffusivities show that diffusion-related activities are higher in Fe−Mn alloy than in Fe−Co alloy. Also, as reflected by the plots of viscosity, the viscosities of Fe−Mn and Fe−Co alloys show negative deviations from the Arrhenius' law. The negative deviation is more pronounced in Fe−Co alloy.

Calculations of surface properties indicate that the surface of Fe−Mn alloy is enriched with Mn-atoms while the surface of Fe−Co alloy has almost equal concentrations of iron (Fe) and cobalt (Co) atoms. This indicates that Fe−Co alloy has more Fe-atoms at the surface than Fe−Mn alloy. This possibly suggests that Fe−Mn alloy will be more resistant to corrosion than Fe−Co alloy. The study further shows that the surface tension increases in Fe−Mn alloy with increasing bulk concentration of iron (Fe). On the other hand, the surface tension of Fe−Co alloy decreases to around 0.59 atomic fraction of iron (Fe) before it rises rapidly with increasing bulk concentration of iron (Fe). The results of surface $S_{cc}(0)$ for the two liquid alloys corroborate the results of bulk properties calculations.

5.2 Recommendation

The results of this work have shown that for liquid Fe−Co alloy, the self-association model of Singh and Sommer (1992) could not reproduce quantitatively the experimental Gibbs free energy of mixing, activity, and bulk $S_{cc}(0)$. Therefore, it is suggested that other theoretical models could be used to study the properties of this important alloy.

5.3 Contribution to knowledge

The experimental values of self-diffusivities, surface tension and viscosity of the components of the two liquid alloys studied at 1863 K are not available in the literature. Calculations in this work have been able to predict to a reasonable extent the values of these quantities for iron (Fe), manganese (Mn) and cobalt (Co) at 1863 K.

REFERENCES

Ajayi, A. A., Ogunmola, E. D., & Adeoye, A. E. (2017). Chemical Ordering in Na-Pb and Na-Hg Liquid Alloys. *American Journal of Condensed Matter Physics*, *7* (3), 67–72.

Akinlade, O., Boyo, A. O., & Ijaduola, B. R. (1999). Demixing tendencies in somes Sn-based liquid alloys. *Journal of Alloys and Compounds*, *290*, 191–196.

Akinlade, O., & Singh, R. N. (2002). Bulk and surface properties of liquid In – Cu alloys. *Journal of Alloys and Compounds*, *333*, 84–90.

Anusionwu, B. C. (2003). Surface properties of some sodium-based binary liquid alloys. *Journal of Alloys and Compounds*, *359*, 172–179.

Anusionwu, B. C., Adebayo, G. A., & Mbamala, E. C. (2013). Intermetallics and Thermophysical Properties of Liquid Ag-La and Ag-Pr Alloys. *The African Review of Physics*, *8* (7), 39–49.

Anusionwu, B. C., Akinlade, O., & Hussain, L. A. (1998). Assessment of size effect on the surface properties of some binary liquid alloys. *Journal of Alloys and Compounds*, *278*, 175–181.

Anusionwu, B. C., & Echendu, O. K. (2010). Thermodynamic studies of the surface and transport properties in Ag – In and Ag – Sb liquid alloys. *Physics and Chemistry of Liquids*, *48* (1), 127–140.

Anusionwu, B. C., Madu, C. A., & Orji, C. E. (2009). Theoretical studies of mutual diffusivities and surface properties in Cd – Ga liquid alloys. *PRAMANA-Journal of Physics*, *72* (6), 951–967.

Bhatia, A. B., Hargrove, W. H., & March, N. H. (1973). Concentration fluctuations in conformal solution and partial structure factor in alloys. *J. Phys. C: Solid State Physics*, *6*, 621.

Bhatia, A. B., Hargrove, W. H., & Thornton, D. E. (1974). Concentration fluctuations and partial structure factors of compound-forming binary molten alloys. *Phys. Rev. B*, *9* (2), 435–444.

Bloch, F., Waeckerle, T., & Fraisse, H. (2007). The use of iron-nickel and iron-cobalt alloys in electrical engineering, and especially for electrical motors. In *Electrical Insulation conference and Electrical Manufacturing Expo*.

Boyo, A. O. (2005). The study of thermodynamic properties of liquid NaCs alloys. *AJST*, *6* (1), 73–79.

Bramhall, M. D. (1989). *The impact toughness of iron manganese alloys*. Dissertation, Sheffield Hallam University, United Kingdom. Retrieved from http://shura.shu.ac.uk/19392/

Butler, J. A. V. (1932). Thermodynamic of surface solution. *Proc. R. Soc. A*, *135*, 348.

Charles, J., & Issi, J. P. (1984). Electrical and thermal conductivities of Fe-Mn-Al austenitic alloys. *J. Phys. D: Appl. Phys.*, *17*, 2399–2406.

Cobalt. (n.d.). Retrieved January 2, 2019, from https://en.m.wikipedia.org/wiki/Cobalt

Couto, A. A., & Ferreira, P. I. (1989). Phase transformations and properties of Fe-Co alloys. *J. Mater. Eng.*, *11*, 31–36.

Cowley, J. M. (1950). An Approximate Theory of Order in Alloys. *Phys. Rev.*, *77* (5), 669–675.

Dalgic, S., & Colakogullari, M. (2006). Self-diffusion coefficients in liquid Ag using the embedded atom model based effective pair potentials. *Turk J Phys*, *30*, 303–310.

Darken, L. S. (1948). Diffusion , Mobility and Their Interrelation through Free Energy in Binary Metallic Systems. *Trans. AIME*, *175*, 184.

Downing, J. H. (n.d.). Manganese processing. Retrieved December 19, 2018, from https://www.britannica.com/technology/manganese-processing

Drynda, A., Hassel, T., Wilhelm, B. F., & Peuster, M. (2014). In vitro and in vivo corrosion properties of new iron – manganese alloys designed for cardiovascular applications. *J Biomed Mater Res Part B 2014*, *00B*, 000–000.

Elmen, G. W. (1929). *1739752*. U.S Patent.

Faber, T. E. (1972). *Introduction to the theory of liquid metals*. Cambridge University Press.

Fingers, R. T., & Kozlowski, G. (1997). Microstructure and magnetic properties of Fe – Co alloys. *Journal of Applied Physics*, *81* (8), 4110–4111. https://doi.org/10.1063/1.365095

Flory, J. (1942). Thermodynamics of high polymer solutions. *J. Chem. Phys.*, *10*, 51.

Gasior, W., Fima, P., & Moser, Z. (2011). Modeling of the thermodynamic properties of liquid Fe-Ni and Fe-Co alloys from the surface tension data. *Arch. Metall. Mater*, *56* (1), 13–23.

Gould, H. L. B., & Wenny, D. H. (1956). Supermendur, a new rectangular loop magnetic material with high magnetic flux density and low coercive force. In *Conference on magnetism and magnetic material, 2nd*. Boston, MA.

Grosse, A. V. (1961). The viscosity of liquid metals and an empirical relationship between their activation energy of viscosity and their melting points. *J. Inorg. Nucl. Chem.*, *23*, 333–339.

Guggenheim, E. A. (1952). *Mixture*. Oxford University Press, London.

Gurrappa, I. (2002). Corrosion studies related to suitability of permanent magnets for biomedical applications. *Mater Charact*, *48*, 63–70.

Hermawan, H., Alamdari, H., Mantovani, D., & Dube, D. (2008). Iron – manganese : new class of metallic degradable biomaterials prepared by powder metallurgy. *Powder Metallurgy*, *51* (1), 38–45.

Hermawan, H., Purnama, A., Dube, D., Couet, J., & Mantovani, D. (2010). Fe – Mn alloys for metallic biodegradable stents : Degradation and cell viability studies. *Acta Biomaterialia*, *6*, 1852–1860.

Hultgren, R., Desai, P. D., Hawkins, D. T., Gleiser, M., & Kelly, K. K. (1973). *Selected values of the thermodynamic properties of binary alloys*. Ohio, USA: American Society for Metals.

Iida, T., & Guthrie, R. I. L. (1988). *The Physical properties of liquid metals*. Oxford: Clarendon Press.

Iida, T., Morita, Z., & Takuchi, S. (1975). Viscosity measurements of pure liquid metals by the capillary method. *Institute of Metals and Materials*, *39* (11), 1169–1175.

Iron-Cobalt (Fe-Co) Phase Diagram. (n.d.). Retrieved January 1, 2019, from www.calphad.com/iron-cobalt.html

Iron-Manganese (Fe-Mn) Phase Diagram. (n.d.). Retrieved January 1, 2019, from www.calphad.com/iron-manganese.html

Kaptay, G. (2005). A unified equation for the viscosity of pure liquid metals. *Z. Metallkd.*, *96*, 1–8.

Koirala, I., Jha, I. S., & Singh, B. P. (2014). Theoretical investigation on ordering nature of Cd-Bi alloys in the molten state. *BIBECHANA*, *11* (1), 70–78.

Koirala, I., Singh, B. P., & Jha, I. S. (2014). Transport and Surface Properties of Molten Cd-Zn Alloys. *Journal of Institute of Science and Technology*, *19* (1), 14–18.

Koirala, R. P., Kumar, J., Singh, B. P., & Adhikari, D. (2014). Bulk and surface properties of Co – Fe and Fe – Pd liquid alloys. *Journal of Non-Crystalline Solids*, *394–395*, 9–15.

Koirala, R. P., Singh, B. P., Jha, I. S., & Adhikari, D. (2013). Thermodynamic, structural and surface properties of liquid Cd – Zn alloys. *Journal of Molecular Liquids*, *179*, 60–66.

Laty, P., Joud, J. C., & Desre, P. (1976). Surface tensions of binary liquid alloys with strong chemical interactions. *Surface Science*, *60*, 109–124.

Lee, S., Han, J., Lee, S., Kang, S., Lee, S., & Lee, Y. (2017). Design for Fe-high Mn alloy with an improved combination of strength and ductility. *Scientific Reports*, *7*, 3573.

Liquid. (n.d.). Retrieved January 2, 2019, from https://en.m.wikipedia.org/wiki/Liquid

Liu, S., Bauser, S., Turgut, Z., Coate, J., & Fingers, R. T. (2003). Fe – Co – V alloy with improved magnetic properties and high-temperature creep resistance. *J. Appl. Phys.*, *93* (10), 7118–7120.

Manganese. (n.d.). Retrieved December 19, 2018, from www.britannica.com/science/manganese

Mathieu, J. B., Martel, S., Yahia, L. H., Soulez, G., & Beaudoin, G. (2005). Preliminary investigation of the feasibility of magnetic propulsion for future microdevices in blood vessels. *Bio-Medical Mater Eng*, *15*, 367–374.

Moelwyn-Hughes, E. A. (1961). *Physical chemistry*. Oxford: Permagon press.

Nasim, M. (1979). *Brittleness in ferritic Fe-Mn alloys*. Dissertation, Sheffield Hallam University, United Kingdom. Retrieved from http://shura.shu.ac.uk/20109/

Novakovic, R. (2010). Thermodynamics, surface properties and microscopic functions of liquid Al-Nb and Nb-Ti alloys. *J. Non-Cryst. Solids*, *356*, 1593.

Novakovic, R. (2011). Bulk and surface properties of liquid Al – Cr and Cr – Ni alloys. *J. Phys.: Condens. Matter*, *23* (235107), 8.

Novakovic, R., Giuranno, D., Ricci, E., Tuissi, A., Wunderlich, R., Fecht, H., & Egry, I. (2012). Surface , dynamic and structural properties of liquid Al – Ti alloys. *Applied Surface Science*, *258*, 3269–3275.

Odusote, Y. A., & Popoola, A. I. (2017). Thermodynamic and Surface Properties of Cr-X , (X = Mo , Fe) Liquid Alloys. *American Journal of Condensed Matter Physics*, *7* (3), 57–66.

Opiela, M., Grajcar, A., & Krukiewicz, W. (2009). Corrosion behaviour of Fe-Mn-Si-Al austenitic steel in chloride solution, *33* (2), 159–165.

Periodic table. (n.d.). Retrieved December 19, 2018, from www.rsc.org/periodic-table/element/26/iron

Pouponneau, P., Savadogo, O., Napporn, T., Yahia, L., & Martel, S. (2010). Corrosion Study of Iron-Cobalt Alloys for MRI-Based Propulsion Embedded in Untethered Microdevices Operating in the Vascular Network. *Journal of Biomedical Materials Research Part B: Applied Biomaterials*, 203–211.

Prasad, L. C., & Singh, R. N. (1991). Surface segregation and concentration fluctuations at the liquid-vapor interface of molten Cu-Ni alloys. *Phys. Rev. B, 44* (24), 13768–13771.

Prasad, L. C., Singh, R. N., & Singh, G. P. (1994). The Role of Size Effects on Surface Properties. *Phys. Chem. Liq.*, *27*, 179–185.

Prasad, L. C., Singh, R. N., Singh, V. N., & Chatterjee, S. K. (1995). Compound formation in Sn-based liquid alloys. *Physica B*, *215*, 225–232.

Prasad, L. C., Singh, R. N., Singh, V. N., & Singh, G. P. (1998). Correlation between Bulk and Surface Properties of AgSn Liquid Alloys. *J. Phys. Chem. B*, *102*, 921–926.

Preuss, A. (1912). *Dissertation*, University of Zurich.

Protopapas, P., Andersen, H. C., & Parlee, N. A. D. (1973). Theory of transport in liquid metals . I . Calculation of selfdiffusion coefficients. *J. Chem. Phys.*, *59*, 15–25.

Reclaru, L., Luthy, H., Eschler, P. Y., Blatter, A., & Susz, C. (2005). Corrosion behaviour of Cobalt-Chromium dental alloys doped with precious metals. *Biomaterials*, *26*, 4358–4365.

Schwitzgebel, G., & Langen, G. (1981). Application of the Hard Sphere Theory to the Diffusion of Binary Liquid Alloy Systems. *Z. Naturforsch*, *36a*, 1225–1232.

Senk, D., Emmerich, H., Rezende, J., & Siquieri, R. (2007). Estimation of Segregation in Iron-Manganese Steels. *Advanced Engineering Materials*, *9* (8), 695–702.

Singh, R. N. (1987). Short-range order and concentration fluctuations in binary molten alloys. *Can. J. Phys.*, *65*, 309–325.

Singh, R. N., Pandey, D. K., Sinha, S., Mitra, N. R., & Srivastava, P. L. (1987). Thermodynamic properties of molten LiMg alloy. *Physica 145B*, 358–364.

Singh, R. N., & Sommer, F. (1992). Simple model for demixing binary liquid alloys. *Z. Metallkd.*, *83*, 553.

Singh, R. N., & Sommer, F. (1992). Temperature dependence of the thermodynamic functions of strongly interacting liquid alloys. *J. Phys. Condens. Matter*, *4*, 5345–5358.

Singh, R. N., & Sommer, F. (1997). Segregation and immiscibility in liquid binary alloys. *Rep. Prog. Phys.*, *60*, 57–150.

Smithells, C. J., & Brandes, E. A. (1978). *Metals reference book* (5th ed.). Butterworths, London.

Varadaraajan, V. (2015). *Development of a novel iron-manganese alloy and its application*. Dissertation, University of Michigan-Dearborn.

Vasiliev, M. A. (1997). Surface effects of ordering in binary alloys. *J.Phys. D: Appl. Phys.*, *30*, 3037–3070.

Warren, B. E. (1969). *X-ray diffraction*. Addison Wesley, Reading, MA.

Weiss, P. (1912). The magnetic properties of the alloys of the ferromagnetic metals: iron-nickel, nickel-cobalt, cobalt-iron. *Trans. Faraday Soc.*, *8*, 149.

White, J. H., & Wahl, C. V. (1932). *1862599*. U.S Patent.

Yokoyama, I. (1999). Self-diffusion coefficient and its relation to properties of liquid metals: a hard-sphere description. *Physica B*, *271*, 230–234.